

ARTICLE

ASC deglutathionylation is a checkpoint for NLRP3 inflammasome activation

Shuhang Li¹, Linlin Wang², Zhihao Xu⁶, Yuanyuan Huang¹, Rufeng Xue³, Ting Yue⁴, Linfeng Xu⁴, Fanwu Gong⁶, Shiyu Bai¹, Qielan Wu¹, Jiwei Liu¹, Bolong Lin⁶, Huimin Zhang¹, Yanhong Xue², Pingyong Xu², Junjie Hou², Xiaofei Yang⁵, Tengchuan Jin¹, Rongbin Zhou¹, Jizhong Lou², Tao Xu², and Li Bai^{1,6}

Activation of NLRP3 inflammasome is precisely controlled to avoid excessive activation. Although multiple molecules regulating NLRP3 inflammasome activation have been revealed, the checkpoints governing NLRP3 inflammasome activation remain elusive. Here, we show that activation of NLRP3 inflammasome is governed by GSTO1-promoted ASC deglutathionylation in macrophages. Glutathionylation of ASC inhibits ASC oligomerization and thus represses activation of NLRP3 inflammasome in macrophages, unless GSTO1 binds ASC and deglutathionylates ASC at ER, under control of mitochondrial ROS and triacylglyceride synthesis. In macrophages expressing ASC^{C171A}, a mutant ASC without glutathionylation site, activation of NLRP3 inflammasome is GSTO1 independent, ROS independent, and signal 2 less dependent. Moreover, *Asc^{C171A}* mice exhibit NLRP3-dependent hyperinflammation in vivo. Our results demonstrate that glutathionylation of ASC represses NLRP3 inflammasome activation, and GSTO1-promoted ASC deglutathionylation at ER, under metabolic control, is a checkpoint for activating NLRP3 inflammasome.

Introduction

Inflammasomes are key components of innate immune responses against danger signals such as pathogens and dead cells. Activation of inflammasome leads to cleavage-based activation of caspase-1 that induces pyroptosis and processes the proinflammatory cytokines IL-1 β and IL-18 (McKee and Coll, 2020; Miao et al., 2011). NLRP3 inflammasome is the best-studied inflammasome, and its excessive activation relates to autoimmune diseases and inflammatory diseases. Given these consequences, activation of NLRP3 inflammasome is precisely controlled (Schroder and Tschopp, 2010). Activating NLRP3 inflammasome requires priming (signal 1) and activation (signal 2) signals. Activation signal, such as ATP, nigericin, and crystals, promotes assembly of NLRP3 inflammasome and the nucleation of the apoptosis-associated speck-like protein containing a CARD (ASC; Lu et al., 2014; Schroder and Tschopp, 2010). Nucleated ASC proteins recruit pro-caspase-1 and promote its cleavage. In this activation step, ASC oligomerization is an essential process (Dick et al., 2016). Both the N-terminal Pyrin domain and the C-terminal caspase recruitment domain (CARD) are required for ASC oligomerization, with ASC Pyrin domain assembling into

filaments and CARD condensing ASC filaments into specks (Schmidt et al., 2016). ASC oligomerization is regulated by posttranslational modification, including ubiquitination, deubiquitination, and phosphorylation (Chung et al., 2016; Hoss et al., 2017). Whether other mechanisms govern ASC oligomerization and prevent unwanted NLRP3 inflammasome activation remains unclear.

Omega-class glutathione (GSH) transferase 1 (GSTO1) has been reported to promote NLRP3 inflammasome activation and inflammatory diseases

GSTO1 belongs to the glutathione transferase (GST) enzyme family. Different from other GSTs, GSTOs could catalyze thioltransferase reactions as glutaredoxins (Board et al., 2000). Its capability of deglutathionylating protein implicates a role of GSTO1 in protein posttranslational modification (Menon and Board, 2013). Whether GSTO1-catalyzed deglutathionylation contributes to the precise control of ASC oligomerization and NLRP3 inflammasome activation remains unclear.

¹Department of Oncology of the First Affiliated Hospital, School of Basic Medical Sciences, Division of Life Sciences and Medicine, University of Science and Technology of China, Hefei, China; ²Institute of Biophysics, Chinese Academy of Sciences, Beijing, China; ³Department of Obstetrics and Gynecology, the First Affiliated Hospital of Anhui Medical University, Hefei, China; ⁴School of Life Sciences, Division of Life Sciences and Medicine, University of Science and Technology of China, Hefei, China; ⁵College of Biomedical Engineering, South-Central University for Nationalities, Wuhan, China; ⁶Hefei National Laboratory for Physical Sciences at Microscale, School of Basic Medical Sciences, Division of Life Sciences and Medicine, University of Science and Technology of China, Hefei, China.

Correspondence to Li Bai: baili@ustc.edu.cn.

© 2021 Li et al. This article is distributed under the terms of an Attribution–Noncommercial–Share Alike–No Mirror Sites license for the first six months after the publication date (see <http://www.rupress.org/terms/>). After six months it is available under a Creative Commons License (Attribution–Noncommercial–Share Alike 4.0 International license, as described at <https://creativecommons.org/licenses/by-nc-sa/4.0/>).

Here, we show an essential role of GSTO1 in promoting ASC oligomerization and NLRP3 inflammasome activation in macrophages via deglutathionylating ASC. In response to NLRP3 inflammasome activators, GSTO1 binds ASC and promotes ASC deglutathionylation at ER, under control of mitochondrial ROS and triacylglyceride synthesis, respectively (Hughes et al., 2019; Menon et al., 2017). In *Asc^{CIT7A}* macrophages expressing non-glutathionylated ASC protein, activation of NLRP3 inflammasome is GSTO1 independent, ROS independent, and signal 2 less dependent. Moreover, *Asc^{CIT7A}* mice display hyperinflammation upon activating NLRP3 inflammasome in vivo. Altogether, we propose that glutathionylation of ASC inhibits ASC oligomerization, and deglutathionylation of ASC at ER, under metabolic control, is a checkpoint for ASC oligomerization and NLRP3 inflammasome activation in macrophages.

Results

GSTO1 promotes NLRP3 inflammasome activation in macrophages

We generated *Gsto1^{-/-}* mice and confirmed the deletion of GSTO1 protein in *Gsto1^{-/-}* bone marrow-derived macrophages (BMDMs; Fig. 1 A). These *Gsto1^{-/-}* mice were more resistant than *Gsto1^{+/+}* mice in developing NLRP3 inflammasome-dependent arthritis, as indicated by less joint swelling gain (Fig. 1 B) after injecting NLRP3 inflammasome activator monosodium urate (MSU). Moreover, joints from the aforementioned *Gsto1^{-/-}* mice released much less IL-1 β than those joints from control mice when cultured ex vivo (Fig. 1 C). Next, we activated NLRP3 inflammasome in BMDMs in vitro with LPS followed by ATP and found that IL-1 β production was inhibited in *Gsto1^{-/-}* BMDMs (Fig. 1 D). However, IL-6 and TNF- α were not influenced by GSTO1 deficiency. Although *Gsto1^{-/-}* BMDMs produced less mature IL-1 β after activation, they had similar level of pro-IL-1 β as *Gsto1^{+/+}* BMDMs (Fig. 1 E). These results indicated that deficiency of GSTO1 reduced processing of pro-IL-1 β . Moreover, reduced active caspase-1 p20 but normal pro-caspase-1 was detected in *Gsto1^{-/-}* BMDMs (Fig. 1 E), indicating impaired activation of NLRP3 inflammasome. Additionally, we stimulated *Gsto1^{-/-}* and *Gsto1^{+/+}* peritoneal macrophages with LPS followed by distinct NLRP3 inflammasome activators, including ATP, MSU, Nigericin, and imiquimod. ATP, MSU, and Nigericin activate NLRP3 inflammasome in a K⁺-dependent manner (Próchnicki et al., 2016), whereas imiquimod and CL097 activate in a K⁺-independent manner (Groß et al., 2016). Impaired cleavage of pro-IL-1 β and pro-caspase-1 were detected in *Gsto1^{-/-}* peritoneal macrophages (Fig. 1 F) in response to both K⁺-dependent and K⁺-independent NLRP3 inflammasome activators. To further confirm the role of GSTO1 in activating NLRP3 inflammasome, we restored the GSTO1 expression in *Gsto1^{-/-}* BMDMs, and that successfully recovered IL-1 β production (Fig. S1, A and B).

To test whether GSTO1 promoted NLRP3 inflammasome activation in an enzyme activity-dependent manner, we used inhibitor ML175 to inhibit the catalytic activity of GSTO1. ML175 reduced IL-1 β production from LPS-ATP-stimulated BMDMs in a dose-dependent manner, whereas it showed no influence on

IL-6 or TNF- α production (Fig. 1 G). Moreover, we showed that ML175 inhibited cleavage of pro-IL-1 β and pro-caspase-1 in BMDMs stimulated with LPS followed by NLRP3 inflammasome activator ATP, MSU, Nigericin, imiquimod, and CL097, respectively (Fig. 1, H and I). Therefore, the catalytic activity of GSTO1 is required for both K⁺-dependent and K⁺-independent activation of NLRP3 inflammasome.

GSTO1 promotes NLRP3 inflammasome activator-induced ASC oligomerization in macrophages

Next, we studied the role of GSTO1 in regulating expression of NLRP3, NEK7, ASC, and pro-caspase-1, as well as their interactions. Deficiency of GSTO1 (Fig. 2 A) and inhibitor ML175 (Fig. 2 B) showed no influence on the levels of NLRP3, NEK7, ASC, or pro-caspase-1 in LPS-ATP-stimulated BMDMs. Although genetic deficiency and inhibitor exhibited no influence on NLRP3-NEK7 interaction or NLRP3-ASC interaction in LPS-ATP-stimulated BMDMs, they obviously decreased pro-caspase-1-ASC interaction (Fig. 2, A and B), in line with the reduced activation of caspase-1 (Fig. 1, E and H). Given the role of oligomerized ASC in recruiting and activating pro-caspase-1 (Schmidt et al., 2016), we next measured the oligomerization of ASC. We found that ASC oligomerization was disrupted in BMDMs either with deleted *Gsto1* or treated with ML175 (Fig. 2, C and D). Notably, ML175 inhibited ASC oligomerization in LPS-ATP-stimulated *Gsto1^{+/+}* BMDMs but not in LPS-ATP-stimulated *Gsto1^{-/-}* BMDMs (Fig. 2 E), confirming that ML175 inhibited ASC oligomerization via targeting on GSTO1. Additionally, when ATP, MSU, Nigericin, and imiquimod were used to activate NLRP3 inflammasome in LPS-stimulated peritoneal macrophages, ASC oligomerization was inhibited by deficiency of GSTO1 as well (Fig. 2 F). These results demonstrate that catalytic activity of GSTO1 promotes ASC oligomerization during the activation of NLRP3 inflammasome.

De glutathionylation of ASC by GSTO1 promotes ASC oligomerization in NLRP3 inflammasome

We found that ASC coimmunoprecipitated with GSTO1 at a low level in BMDMs, and LPS-ATP stimulation significantly increased their interaction (Fig. 3 A). Next, we investigated whether GSTO1 could deglutathionylate ASC. ASC was coimmunoprecipitated with antibody against GSH, indicating glutathionylation of ASC (Fig. 3 B). LPS-ATP stimulation reduced the level of glutathionylated ASC in BMDMs (Fig. 3 B), in company with an increase of GSTO1-ASC interaction (Fig. 3 A). GSTO1 deficiency increased the level of glutathionylated ASC in both stimulated and unstimulated BMDMs, suggesting that GSTO1 promoted ASC deglutathionylation in both resting and activated cells (Fig. 3 B). The result that GSTO1 could constitutively deglutathionylate ASC protein in unstimulated BMDMs is in line with the low level of GSTO1-ASC interaction in unstimulated BMDMs. The LPS-ATP stimulation-induced reduction of glutathionylated ASC in *Gsto1^{-/-}* BMDMs implied participation of other factors in mediating ASC deglutathionylation. In all conditions, we found no glutathionylated NLRP3 or glutathionylated pro-caspase-1. Although we detected glutathionylated NEK7, neither LPS-ATP stimulation nor GSTO1 deficiency influenced its glutathionylation. Therefore, the GSTO1

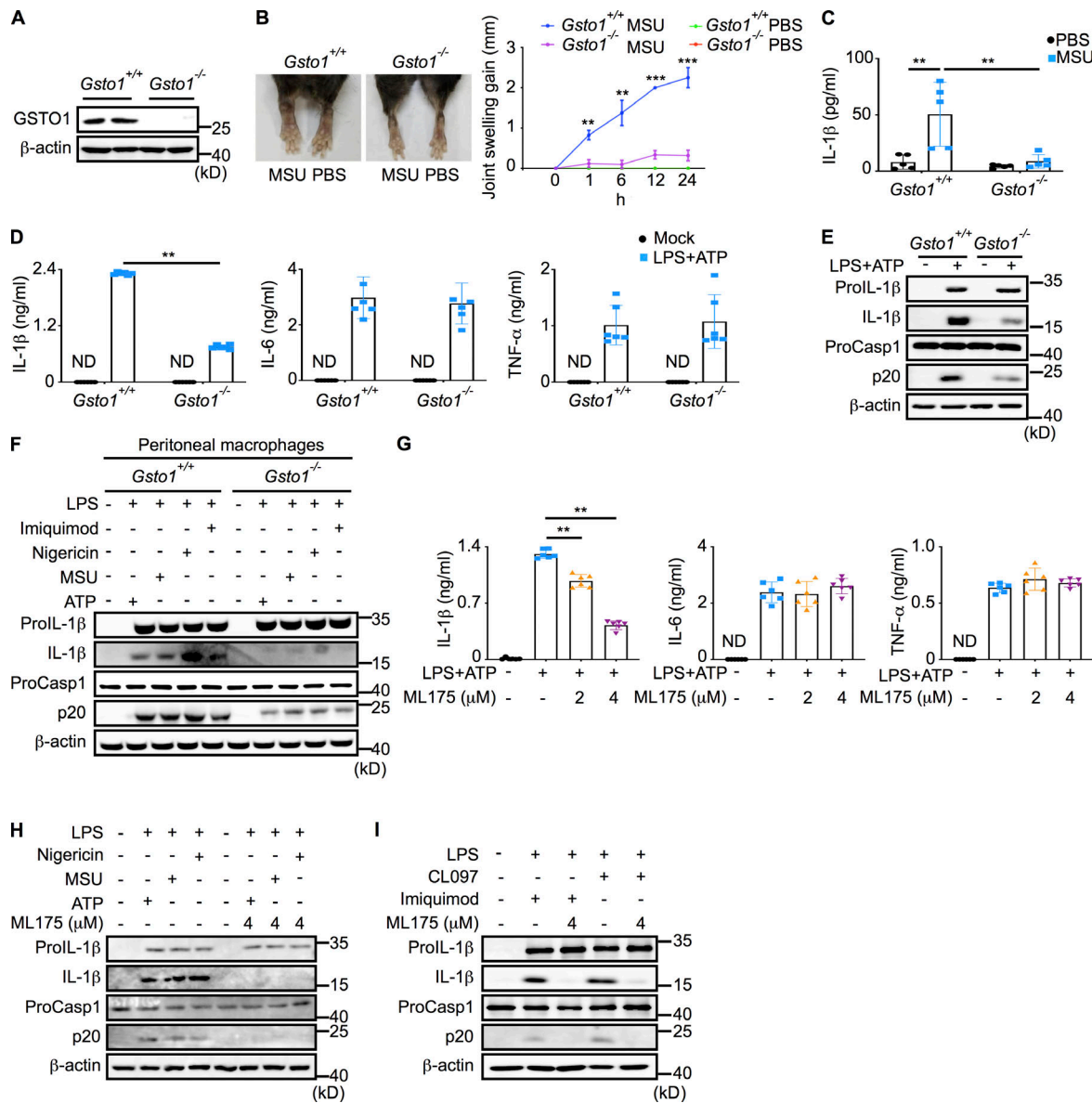


Figure 1. GSTO1 deficiency inhibits activation of NLRP3 inflammasome. (A) Immunoblot analysis for GSTO1 in *Gsto1*^{+/+} and *Gsto1*^{-/-} BMDMs. **(B)** Picture of joints and the joint swelling gain of *Gsto1*^{+/+} and *Gsto1*^{-/-} mice at indicated time points after MSU or PBS injection (*n* = 5 mice; **, *P* < 0.01; ***, *P* < 0.001 by two-tailed Mann–Whitney *U* test). **(C)** IL-1β from joints of *Gsto1*^{+/+} or *Gsto1*^{-/-} mice as described in B (*n* = 5 mice; **, *P* < 0.01 by two-tailed Mann–Whitney *U* test). **(D)** IL-1β, IL-6, and TNF-α production from LPS-ATP-stimulated *Gsto1*^{+/+} and *Gsto1*^{-/-} BMDMs (*n* = 6 samples, representing three independent experiments; ND, not detected; **, *P* < 0.01 by two-tailed Mann–Whitney *U* test). **(E and F)** Immunoblot analysis for pro-IL-1β, cleaved IL-1β, pro-caspase-1, and active caspase-1 p20 in *Gsto1*^{+/+} and *Gsto1*^{-/-} BMDMs (E) and peritoneal macrophages (F), stimulated with LPS and indicated NLRP3 inflammasome activators. **(G)** IL-1β, IL-6, and TNF-α production from LPS-ATP-stimulated BMDMs treated with ML175 at indicated concentrations (*n* = 6 samples, representing three independent experiments; ND, not detected; **, *P* < 0.01 by two-tailed Mann–Whitney *U* test). **(H and I)** Immunoblot analysis for pro-IL-1β, cleaved IL-1β, pro-caspase-1, and active caspase-1 p20 in BMDMs stimulated with LPS followed by ATP, MSU, or Nigericin (H) or followed by CL097 or imiquimod (I) in the presence or absence of ML175. Data are representative of at least three independent experiments (A, E, F, H, and I).

promotes deglutathionylation of ASC but not other NLRP3 inflammasome components.

ASC protein has only one cysteine residue at position 171, which is the potential glutathionylation site. Next, we generated *Asc*^{C171A} mice, in which the *Asc*^{C171A} protein could not be glutathionylated due to the substitution of alanine for cysteine. In coimmunoprecipitation experiments, we detected no ASC glutathionylation in *Asc*^{C171A} BMDMs (Fig. 3 C). To further confirm the glutathionylation of ASC at cysteine¹⁷¹ and reveal the

glutathionylated ASC in situ, we performed proximity ligation assay (PLA), in which two PLA probe-labeled secondary antibodies bound the primary antibodies against ASC and GSH and generated fluorescence signal only if ASC was posttranslationally modified by glutathionylation. This imaging-based assay revealed glutathionylated ASC protein in *Asc*^{wt} BMDMs but not *Asc*^{C171A} BMDMs, further confirming the glutathionylation of ASC at cysteine¹⁷¹ in unstimulated cells (Fig. 3, D and E). Consistently, LPS-ATP stimulation reduced the amount of glutathionylated ASC

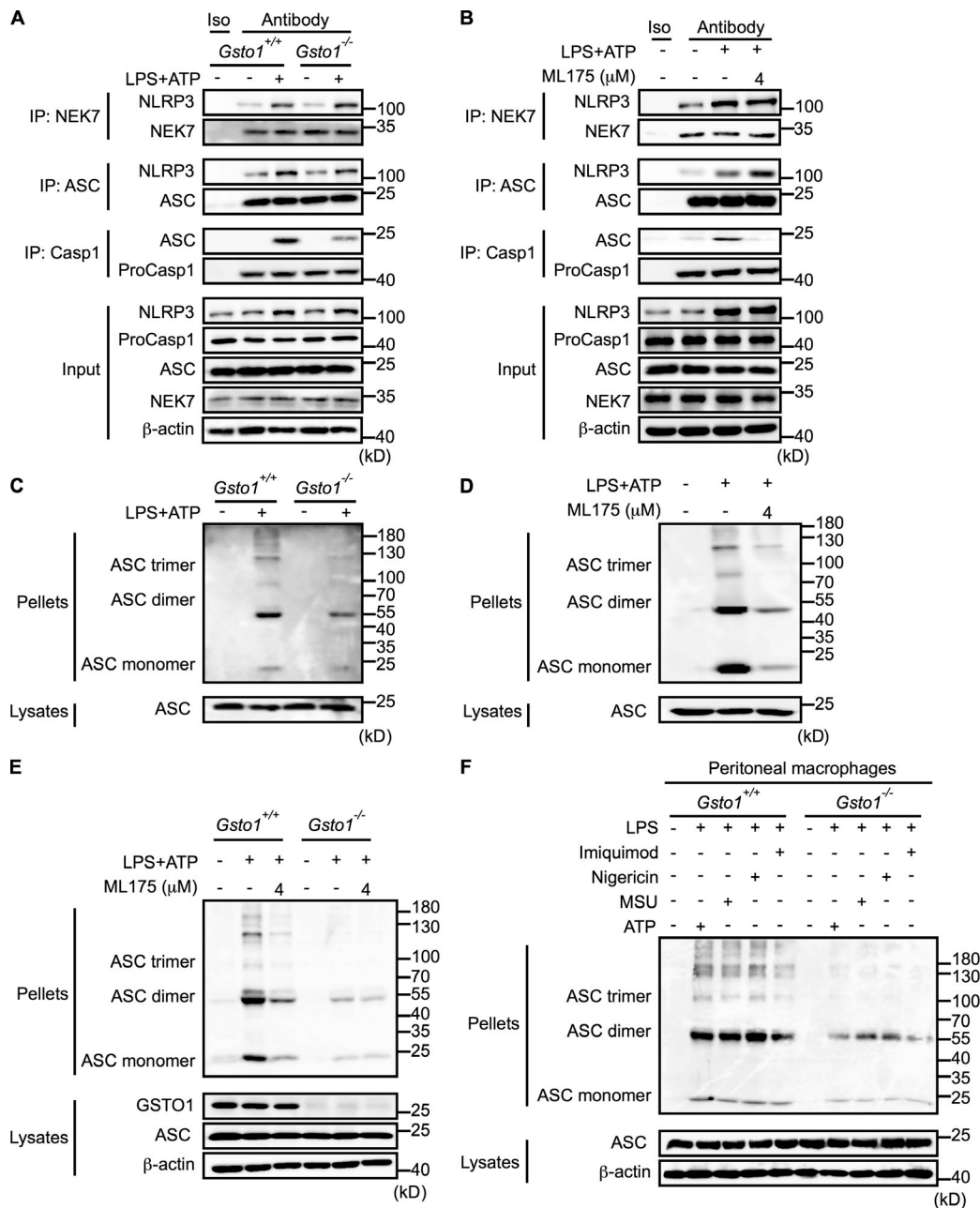


Figure 2. GSTO1 promotes NLRP3 inflammasome activator-induced ASC oligomerization. (A and B) Coimmunoprecipitation of NEK7 and NLRP3, ASC and NLRP3, and pro-caspase-1 and ASC in unstimulated and LPS-ATP-stimulated BMDMs, with or without deleting *Gsto1* (A) or treated with or without ML175 (B). **(C and D)** Immunoblot analysis for ASC oligomerization in unstimulated and LPS-ATP-stimulated BMDMs, with or without deleting *Gsto1* (C) or treated with or without ML175 (D). **(E and F)** Immunoblot analysis for ASC oligomerization in unstimulated or LPS-ATP-stimulated *Gsto1*^{+/+} and *Gsto1*^{-/-} BMDMs with or without ML175 (E) and in *Gsto1*^{+/+} and *Gsto1*^{-/-} peritoneal macrophages stimulated with LPS followed by ATP, MSU, Nigericin, or imiquimod (F). Data are representative of at least three independent experiments (A–F).

in *Asc*^{wt} BMDMs, as indicated by reduced ASC-GSH PLA puncta numbers, and ML175 restored the amount of glutathionylated ASC (Fig. 3, D and E). These results further prove the role of GSTO1 in deglutathionylating ASC in activated BMDMs. Additionally, we compared the numbers of ASC-GSH PLA puncta in *Gsto1*^{+/+} and *Gsto1*^{-/-} peritoneal macrophages. Again, we found that GSTO1 deficiency increased the amount of glutathionylated ASC in peritoneal macrophages stimulated with LPS and distinct NLRP3 inflammasome activators, including ATP, MSU, Nigericin, and

imiquimod, as well as in unstimulated peritoneal macrophages (Fig. 3 F). These results further support that GSTO1 promotes ASC deglutathionylation in response to distinct NLRP3 inflammasome activators in macrophages.

Molecular dynamics (MD) simulations showed that residue cysteine¹⁷¹ localized at the ASC-CARD multimerization interface (Fig. S2 A). GSH covalently linking to cysteine¹⁷¹ at the interface clashed with the other ASC-CARD domain (Fig. S2 B). Additionally, binding of GSH at cysteine¹⁷¹ caused domain rotation

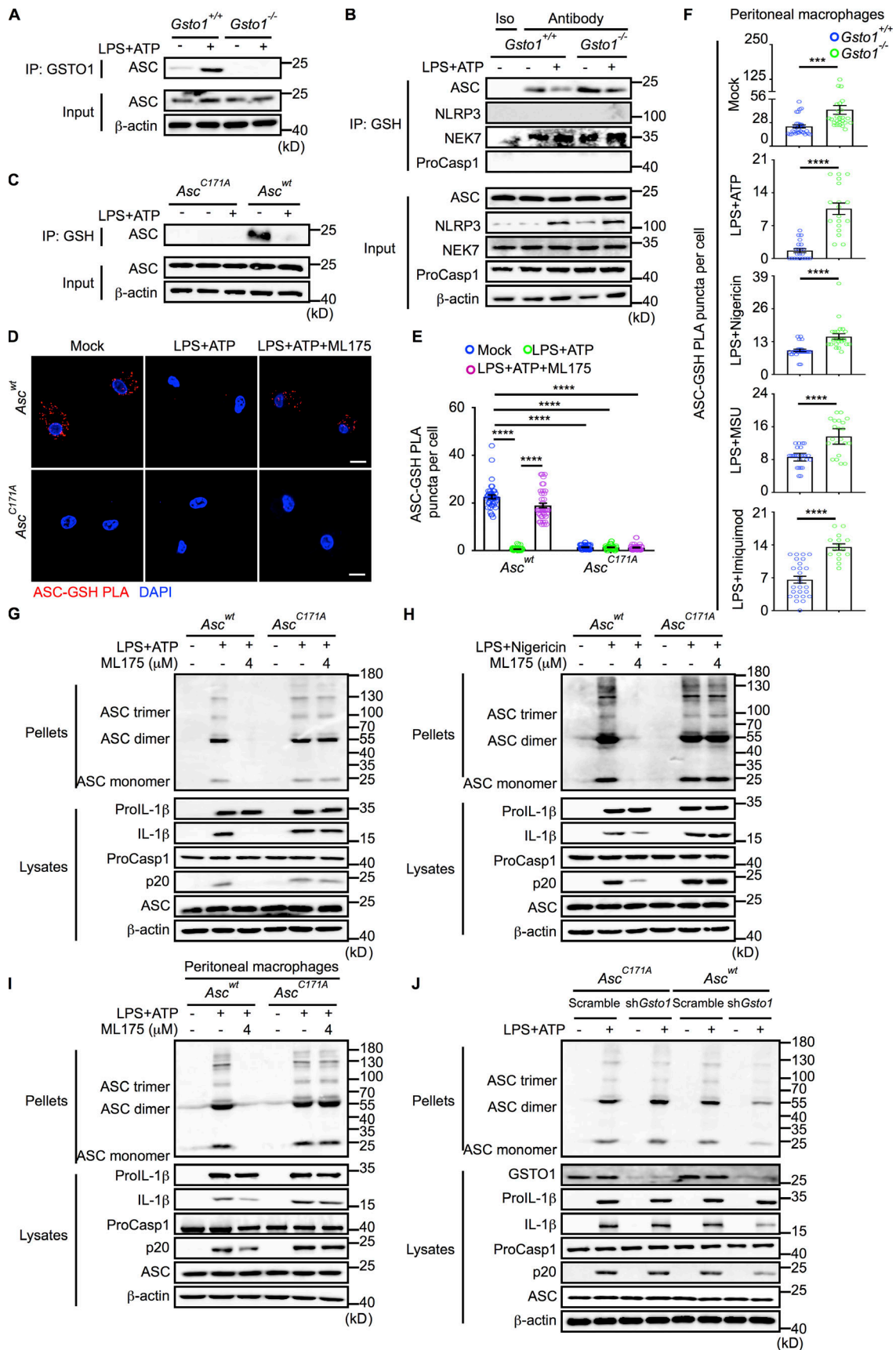


Figure 3. **GSTO1 promotes NLRP3 inflammasome activation by deglutathionylating ASC at cysteine¹⁷¹.** (A) Coimmunoprecipitation of ASC and GSTO1 in *Gsto1*^{+/+} and *Gsto1*^{-/-} BMDMs, with or without LPS-ATP stimulation. (B) Immunoblot analysis for glutathionylation of ASC, NLRP3, NEK7, and pro-caspase-1 in

Gsto1^{+/+} and *Gsto1*^{-/-} BMDMs, with or without LPS-ATP stimulation. **(C)** Immunoblot analysis for glutathionylation of ASC in *Asc*^{wt} and *Asc*^{C171A} BMDMs, with or without LPS-ATP stimulation. **(D)** Glutathionylated ASC (ASC-GSH PLA) in unstimulated *Asc*^{wt} and *Asc*^{C171A} BMDMs, and in LPS-ATP-stimulated *Asc*^{wt} and *Asc*^{C171A} BMDMs, with or without ML175 treatment. Scale bars, 10 μ m. **(E)** Numbers of ASC-GSH PLA puncta in cells described in D ($n = 41$ – 60 cells from three independent experiments; ****, $P < 0.0001$ by unpaired Student's t test). **(F)** Numbers of ASC-GSH PLA puncta in *Gsto1*^{+/+} and *Gsto1*^{-/-} peritoneal macrophages with or without stimulation by indicated NLRP3 inflammasome activators ($n = 15$ – 30 cells from three independent experiments; ***, $P < 0.001$; ****, $P < 0.0001$ by unpaired Student's t test). **(G–J)** Immunoblot analysis for ASC oligomerization, pro-IL-1 β , cleaved IL-1 β , pro-caspase-1, and active caspase-1 p20 in ML175 treated or untreated *Asc*^{wt} or *Asc*^{C171A} BMDMs (G and H) and peritoneal macrophages (I) stimulated with indicated NLRP3 inflammasome activators, and in LPS-ATP-stimulated *Asc*^{wt} and *Asc*^{C171A} BMDMs with or without knockdown of *Gsto1* (J). Data are representative of at least three independent experiments (A–D and G–J).

and reduced area of CARD–CARD binding interface in dimeric and 16mer filament simulations (Fig. S2, C–H). These results indicate that GSH conjugation impairs ASC–CARD assembly. Assembly of ASC–CARD domains is required for ASC oligomerization and nucleation of pro-caspase-1 (Dick et al., 2016; Li et al., 2018). Therefore, deglutathionylating ASC at cysteine¹⁷¹ by GSTO1 would promote assembly of ASC–CARD domains and ASC oligomerization as a result. Notably, when extra GSH was added to ML175-treated BMDMs, it reduced the level of glutathionylated ASC and rescued the ASC oligomerization and ASC–pro-caspase-1 interaction (Fig. S3, A–C). To further investigate the role of GSTO1-mediated ASC deglutathionylation in activating NLRP3 inflammasome, we inhibited GSTO1 function with ML175 in *Asc*^{C171A} BMDMs and *Asc*^{C171A} peritoneal macrophages. We found that although ML175 inhibited oligomerization of ASC and processing of pro-caspase-1 and pro-IL-1 β in LPS-ATP-stimulated *Asc*^{wt} BMDMs, LPS-Nigericin-stimulated *Asc*^{wt} BMDMs, and LPS-ATP-stimulated *Asc*^{wt} peritoneal macrophages, ML175 showed no effect in *Asc*^{C171A} BMDMs or *Asc*^{C171A} peritoneal macrophages activated by the above NLRP3 inflammasome activators (Fig. 3, G–I). Moreover, we showed that knockdown of *Gsto1* reduced LPS-ATP stimulation-induced oligomerization of ASC and processing of pro-caspase-1 and pro-IL-1 β in *Asc*^{wt} BMDMs but exhibited no influence in *Asc*^{C171A} BMDMs (Fig. 3 J). These results indicate that, given no ASC glutathionylation, GSTO1 catalytic activity is not required for ASC oligomerization and NLRP3 inflammasome activation in macrophages. In comparison with GSTO1 activity-impaired *Asc*^{wt} macrophages, GSTO1 activity-impaired *Asc*^{C171A} macrophages showed higher levels of ASC oligomerization and increased processing of pro-caspase-1 and pro-IL-1 β after stimulation with LPS and NLRP3 inflammasome activators (Fig. 3, G–J), supporting the inhibitory effect of ASC glutathionylation on activation of NLRP3 inflammasome. Together, our results demonstrate that glutathionylation of ASC represses NLRP3 inflammasome activator-induced ASC oligomerization, and GSTO1 promotes NLRP3 inflammasome activation by deglutathionylating ASC.

ROS promotes GSTO1–ASC interaction and leads to ASC deglutathionylation in response to NLRP3 inflammasome activator

Mitochondrial ROS is known to trigger NLRP3 inflammasome assembly (Sánchez-Rodríguez et al., 2021). We found that LPS-ATP stimulation induced ASC–GSTO1 interaction in BMDMs, as indicated by coimmunoprecipitation of ASC and GSTO1, and this interaction was inhibited by Mito-TEMPO, a mitochondria-targeted antioxidant, in a dose-dependent manner (Fig. 4 A).

We further employed a PLA approach to view the GSTO1–ASC interaction in situ. *Asc*^{-/-} BMDMs were used as negative controls and showed no signal. We confirmed that LPS-ATP stimulation increased GSTO1–ASC interaction in BMDMs, whereas Mito-TEMPO inhibited the ASC–GSTO1 interaction (Fig. 4, B and C). Consequently, the level of ASC that coimmunoprecipitated with GSH increased with Mito-TEMPO treatment in a dose-dependent manner in LPS-ATP-stimulated BMDMs (Fig. 4 D). Additionally, in situ imaging of glutathionylated ASC by a PLA approach further confirmed that Mito-TEMPO treatment increased the level of glutathionylated ASC in LPS-ATP-stimulated BMDMs (Fig. 4, E and F). When another inhibitor, MitoQ, was used to inhibit mitochondrial ROS in LPS-ATP-stimulated BMDMs, similar reduction of ASC–GSTO1 interaction and elevation of glutathionylated ASC were observed (Fig. 4, G and H). On the other hand, EN460, which inhibits generation of ER ROS, showed no influence on ASC–GSTO1 interaction or ASC deglutathionylation (Fig. 4, G and H). Together, these results demonstrate that mitochondrial ROS promotes ASC–GSTO1 interaction and thus enhances GSTO1-mediated ASC deglutathionylation.

Moreover, mitochondrial ROS inhibitors Mito-TEMPO and MitoQ inhibited ASC oligomerization and processing of pro-caspase-1 and pro-IL-1 β in LPS-ATP-stimulated *Asc*^{wt} BMDMs, but exhibited no effect in LPS-ATP-stimulated *Asc*^{C171A} BMDMs (Fig. 4, I and J). Notably, when NLRP3 inhibitor Oridonin was added to LPS-ATP-stimulated *Asc*^{C171A} BMDMs together with Mito-TEMPO, the ASC oligomerization and the processing of pro-caspase-1 and pro-IL-1 β were completely inhibited (Fig. 4 K), confirming that, in *Asc*^{C171A} BMDMs, LPS-ATP stimulation-induced activation of inflammasome in the absence of mitochondrial ROS was NLRP3 dependent. Again, EN460, which inhibits generation of ER ROS, exhibited no influence on ASC oligomerization or processing of pro-caspase-1 and pro-IL-1 β in both *Asc*^{wt} BMDMs and *Asc*^{C171A} BMDMs (Fig. 4 L). Our results, that activation of NLRP3 inflammasome is mitochondrial ROS independent in cells without ASC glutathionylation, demonstrate that mitochondrial ROS promotes activation of NLRP3 via induction of ASC deglutathionylation.

GSTO1 deglutathionylates ASC and promotes ASC oligomerization at ER in response to NLRP3 inflammasome activator

To reveal the site for ASC deglutathionylation, we first studied the location of GSTO1. GSTO1 was perfectly colocalized with ER marker Calnexin in BMDMs, indicating its location at ER (Fig. 5 A). Additionally, we found that glutathionylated ASC as shown by a PLA approach was largely colocalized with Calnexin in BMDMs as well (Fig. 5, B and C). In contrast, neither GSTO1 nor

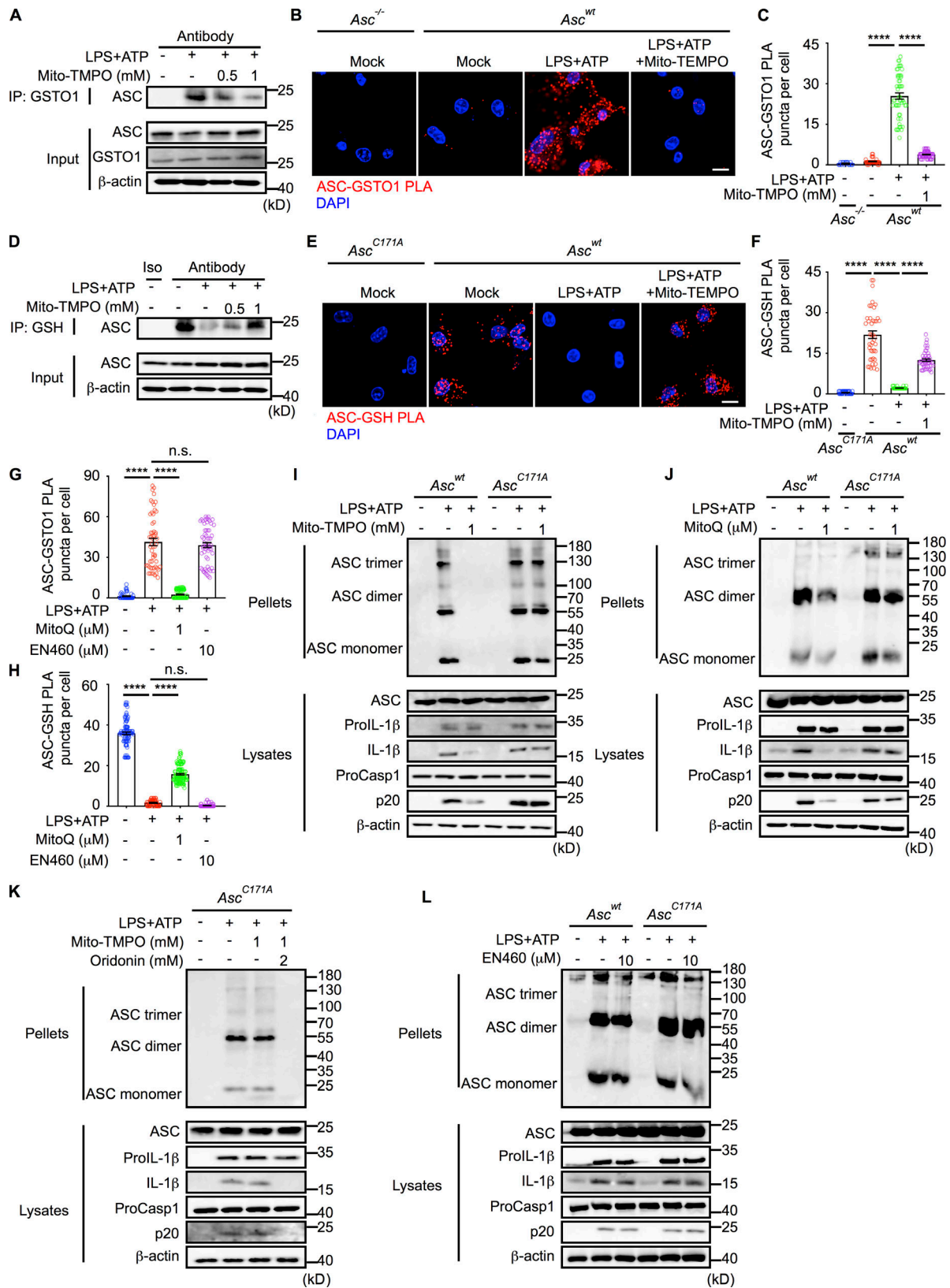


Figure 4. **ROS promotes NLRP3 inflammasome activation via inducing GSTO1-mediated ASC deglutathionylation.** (A and B) Coimmunoprecipitation of ASC and GSTO1 (A) and images of ASC-GSTO1 interaction (ASC-GSTO1 PLA; B) in unstimulated and LPS-ATP-stimulated BMDMs treated with or without Mito-TEMPO at indicated concentrations. *Asc*^{-/-} BMDMs were used as negative controls in B. Scale bars, 10 μm. (C) Numbers of ASC-GSTO1 PLA puncta in cells in B (n = 16–94 cells from three independent experiments; ****, P < 0.0001 by unpaired Student's t test). (D and E) Immunoblot analysis for glutathionylated ASC (D) and images of glutathionylated ASC (ASC-GSH PLA; E) in unstimulated and LPS-ATP-stimulated BMDMs with or without Mito-TEMPO treatment at

indicated concentrations. *Asc*^{C171A} BMDMs were used as negative controls in E. Scale bars, 10 μ m. (F) Numbers of ASC-GSH PLA puncta in cells in E ($n = 37$ –47 cells from three independent experiments; ****, $P < 0.0001$ by unpaired Student's t test). (G and H) Numbers of ASC-GSTO1 PLA puncta (G) and ASC-GSH PLA puncta (H) in unstimulated and LPS-ATP-stimulated BMDMs with or without MitoQ or EN460 treatment at indicated concentrations ($n = 51$ –125 cells from three independent experiments; ****, $P < 0.0001$ by unpaired Student's t test). (I–L) Immunoblot analysis for ASC oligomerization, pro-IL-1 β , cleaved IL-1 β , pro-caspase-1, and active caspase-1 p20 in unstimulated and LPS-ATP-stimulated *Asc*^{wt} and *Asc*^{C171A} BMDMs, treated with or without Mito-TEMPO (I), MitoQ (J), combination of Mito-TEMPO and Oridonin (K), or EN460 (L). Data are representative of at least three independent experiments (A, B, D, E, and I–L).

glutathionylated ASC was colocalized with mitochondrial marker Mito-Tracker (Fig. 5, A–C), although GSTO1 bound ASC in response to mitochondrial ROS (Fig. 4 A). LPS-ATP stimulation led to an increase of GSTO1-ASC interaction, as shown by the PLA approach, and the interaction site also colocalized with Calnexin rather than with Mito-Tracker in BMDMs (Fig. 5, D and E). These results suggest that GSTO1 deglutathionylates ASC, predominantly, at ER. To investigate the location of ASC oligomerization, we separated ER, crude mitochondrial, and cytosolic fractions from BMDMs with or without LPS-ATP stimulation. We found that LPS-ATP stimulation-induced oligomerization of ASC was predominantly detected in ER fraction, with no or a minor amount in the cytosolic or mitochondrial fraction (Fig. 5 F). In line with the role of GSTO1 in promoting ASC oligomerization during the activation of NLRP3 inflammasome, deficiency of GSTO1 reduced LPS-ATP stimulation-induced oligomerization of ASC in ER fraction (Fig. 5 G). Notably, FACLA, a marker for mitochondria-associated ER membranes (MAMs), was detected in the mitochondrial fraction but not in the ER fraction (Fig. 5 F), in line with reported location of MAMs in crude mitochondrial fraction (Wieckowski et al., 2009). Although we could not exclude the possibility that the minor amount of ASC oligomers detected in mitochondrial fraction are related to MAMs, our findings suggest that the majority of ASC oligomers are formed at ER and are not related to MAMs. When Nigericin was used to activate NLRP3 inflammasome in BMDMs, ASC oligomerization was detected predominantly in ER fraction and in a GSTO1-dependent manner as well (Fig. 5, H and I).

To further prove the ER as a site for ASC oligomerization, we viewed the ASC-ASC interaction in situ with a PLA approach, in which two distinct primary antibodies were used to target the different ASC proteins simultaneously, followed by incubation with two PLA probe-labeled secondary antibodies, and only interaction between two ASC proteins binding distinct primary antibodies could generate PLA signal. In *Asc*^{-/-} BMDMs, there was no PLA signal (Fig. 5 J). Although plenty of ASC existed in BMDMs, no PLA signal was detected without stimulation (Fig. 5 J), excluding the possibility that two primary antibodies targeted same ASC protein in unstimulated cells. Additionally, in LPS-ATP-stimulated BMDMs, if two primary antibodies against ASC were added to cells sequentially with an interval long enough to ensure blocking of ASC by the first antibody, we observed no PLA signal (Fig. 5 J). This result indicated that two antibodies competed for binding the same ASC protein, and thereby excluded the possibility of binding two distinct primary antibodies at the same ASC protein in ASC oligomers. In LPS-ATP-stimulated BMDMs, which were stained with two distinct ASC-specific primary antibodies simultaneously, we detected ASC-ASC PLA puncta, and that indicated oligomerization of ASC

(Fig. 5 J). Moreover, these puncta were colocalized with Calnexin rather than with Mito-Tracker (Fig. 5, J and K), further confirming the ER location of ASC oligomerization. In addition to ASC oligomers, LPS-ATP stimulation increased levels of NLRP3 protein in ER fraction from BMDMs (Fig. 5 L). Although LPS-ATP stimulation increased levels of NLRP3 in mitochondrial fraction as well, the level was much lower than in ER fraction. This finding supports the activation of NLRP3 inflammasome at ER.

Triglyceride synthesis in ER promotes ASC deglutathionylation

ER is the major intracellular organelle for lipid synthesis. After LPS-ATP stimulation, BMDMs increased the amount of triacylglyceride (Fig. 6 A) as well as the level of diacylglycerol acyltransferase 1 (DGAT1), a key enzyme for triacylglyceride synthesis (Fig. 6 B). Interestingly, DGAT1 inhibitor T863 reduced LPS-ATP stimulation-induced IL-1 β production from BMDMs (Fig. 6 C). Moreover, we found that T863 did not influence the LPS-ATP stimulation-induced mitochondrial ROS (Fig. 6 D) or GSTO1-ASC interaction (Fig. 6, E and F), but inhibited ASC deglutathionylation, as indicated by increase of glutathionylated ASC in T863-treated BMDMs (Fig. 6, E and F). Moreover, T863 inhibited the oligomerization of ASC and the processing of pro-caspase-1 and pro-IL-1 β in *Asc*^{wt} BMDMs but not in *Asc*^{C171A} BMDMs (Fig. 6 G). These results indicate that T863 interferes with the activation of NLRP3 inflammasome by inhibiting ASC deglutathionylation. To further confirm the functional impact of triacylglyceride synthesis, the key enzyme DGAT1 was knocked down in BMDMs by shRNA. We showed that knockdown of *Dgat1* inhibited oligomerization of ASC, processing of pro-caspase-1 and pro-IL-1 β , and ASC deglutathionylation in *Asc*^{wt} BMDMs, after LPS-ATP stimulation (Fig. 6, H–J). Again, knockdown of *Dgat1* did not influence the LPS-ATP stimulation-induced GSTO1-ASC interaction (Fig. 6, I and J). Due to the absence of ASC glutathionylation in *Asc*^{C171A} BMDMs, knockdown of *Dgat1* in these cells showed no influence on LPS-ATP stimulation-induced oligomerization of ASC or processing of pro-caspase-1 and pro-IL-1 β (Fig. 6 K). Notably, although LPS-ATP stimulation increased the amount of cholesterol, another lipid synthesized in ER as well, inhibiting cholesterol synthesis by Simvastatin showed no influence on IL-1 β production (Fig. S4, A–C). Together, these results demonstrate that triacylglyceride synthesis in ER promotes deglutathionylation of ASC during the activation of NLRP3 inflammasome.

Deglutathionylation of ASC is not required for activating other inflammasomes

In addition to NLRP3 inflammasome, cleavage of pro-caspase-1 and pro-IL-1 β by Pyrin inflammasome, AIM2 inflammasome,

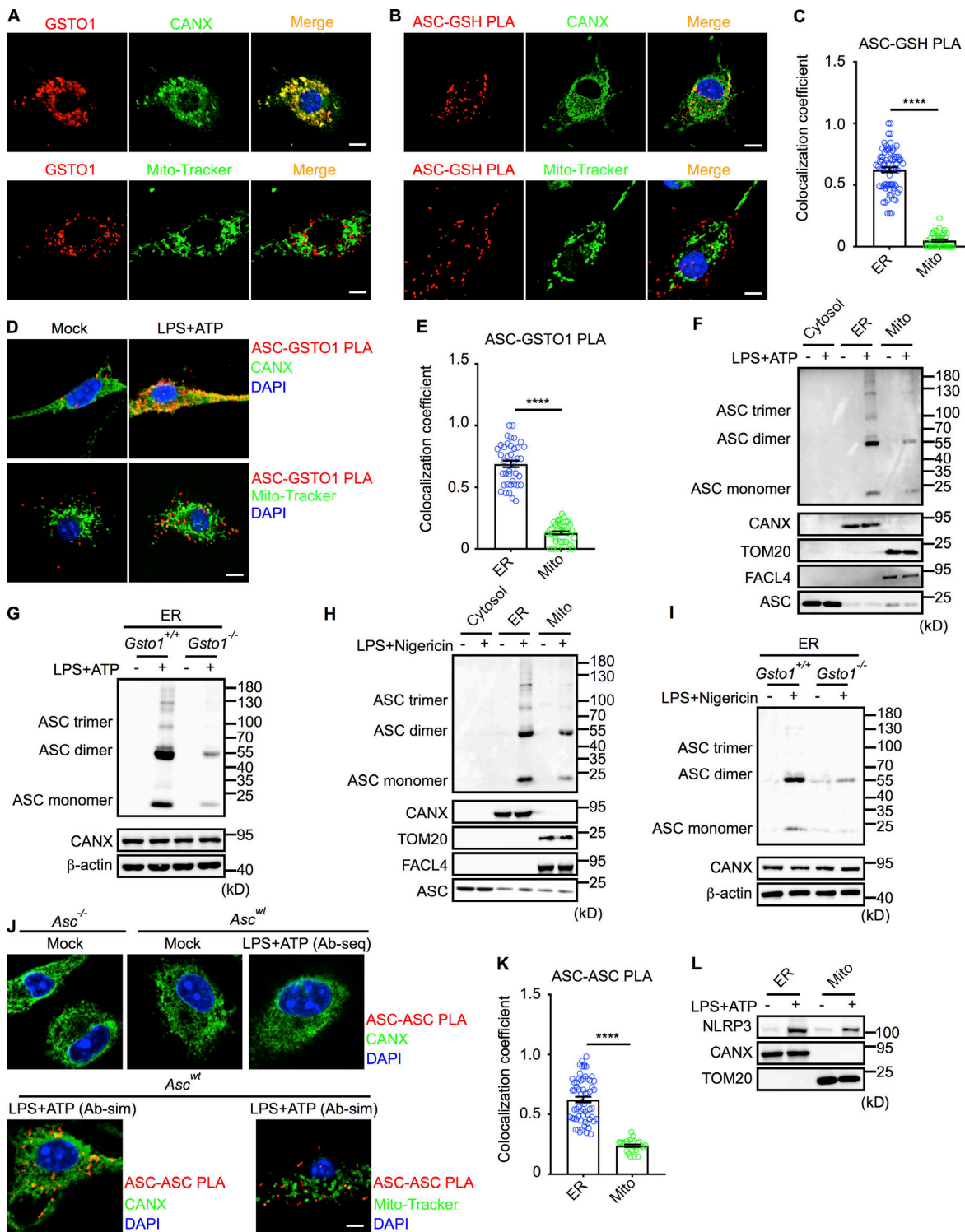


Figure 5. GSTO1 deglutathionylates ASC and promotes ASC oligomerization at ER in response to NLRP3 inflammasome activator. (A) Images of GSTO1, ER marker Calnexin (CANX), and mitochondrial probe Mito-Tracker in BMDMs. Scale bars, 5 μ m. **(B)** Images of CANX, Mito-Tracker, and glutathionylated ASC (ASC-GSH PLA) in BMDMs. Scale bars, 5 μ m. **(C)** Colocalization coefficient of ASC-GSH PLA with CANX or with Mito-Tracker in unstimulated BMDMs ($n = 44$ – 72 cells from three independent experiments; ****, $P < 0.0001$ by unpaired Student's t test). **(D)** Images of CANX, Mito-Tracker, and ASC-GSTO1 interaction (ASC-GSTO1 PLA) in BMDMs with or without LPS-ATP stimulation. Scale bars, 5 μ m. **(E)** Colocalization coefficient of ASC-GSTO1 PLA with CANX or with Mito-Tracker in LPS-ATP-stimulated BMDMs ($n = 40$ cells from three independent experiments; ****, $P < 0.0001$ by unpaired Student's t test). **(F–I)** Immunoblot analysis for ASC oligomerization in cytosolic, ER, and mitochondrial fractions from BMDMs with or without LPS-ATP stimulation (F) or LPS-Nigericin stimulation (H) and in ER fractions from *Gsto1*^{+/+} and *Gsto1*^{-/-} BMDMs with or without LPS-ATP stimulation (G) or LPS-Nigericin stimulation (I). **(J)** Images of CANX, Mito-Tracker, and ASC-ASC interaction (ASC-ASC PLA) in unstimulated and LPS-ATP-stimulated BMDMs. Unstimulated *Asc*^{-/-} and *Asc*^{wt} BMDMs, and LPS-ATP-stimulated *Asc*^{wt} BMDMs stained with two ASC antibodies sequentially (Ab-seq) were used as negative controls for ASC-ASC PLA

staining. Ab-sim, two ASC antibodies were added to cells simultaneously. Scale bars, 10 μm . **(K)** Colocalization coefficient of ASC-ASC PLA with CANX or with Mito-Tracker in LPS-ATP-stimulated BMDMs ($n = 24\text{--}62$ cells from three independent experiments; ****, $P < 0.0001$ by unpaired Student's t test). **(L)** Immunoblot analysis for NLRP3 in ER and mitochondrial fractions from BMDMs with or without LPS-ATP stimulation. Data are representative of three independent experiments (A, B, D, F–J, and L).

and NLR4 inflammasome are ASC dependent (Hornung et al., 2009; Xu et al., 2014; Zhao et al., 2011). Next, we activated Pypin inflammasome, AIM2 inflammasome, and NLR4 inflammasome in BMDMs with LPS-TcdB (*Clostridium difficile* toxin B), LPS-poly(deoxyadenylic-deoxythymidylic [dA:dT]), and LPS-Flagellin, respectively. We found that deficiency of GSTO1 showed no influence on LPS-TcdB stimulation-induced oligomerization of ASC or processing of pro-caspase-1 and pro-IL-1, whereas it diminished LPS-poly(dA:dT) stimulation-induced and LPS-Flagellin stimulation-induced oligomerization of ASC and processing of pro-caspase-1 and pro-IL-1 β (Fig. S5 A). These results demonstrate that GSTO1 is not required for activation of Pypin inflammasome, but it promotes activation of AIM2 inflammasome and NLR4 inflammasome. Notably, the inhibitory effects of GSTO1 deficiency on activation of AIM2 inflammasome and NLR4 inflammasome were less than those on activation of NLRP3 inflammasome. Moreover, *Gsto1* knockdown reduced LPS-poly(dA:dT) stimulation-induced and LPS-Flagellin stimulation-induced oligomerization of ASC and processing of pro-caspase-1 and pro-IL-1 β in both *Asc^{wt}* BMDMs and *Asc^{C171A}* BMDMs similarly (Fig. S5, B and C). Therefore, GSTO1 promotes activation of AIM2 inflammasome and NLR4 inflammasome in an ASC de-glutathionylation-independent manner. Notably, *Gsto1* knockdown *Asc^{wt}* BMDMs and *Gsto1* knockdown *Asc^{C171A}* BMDMs showed similar levels of ASC oligomerization and processing of pro-caspase-1 and pro-IL-1 β in response to LPS-poly(dA:dT) stimulation or LPS-Flagellin stimulation (Fig. S5, B and C), implying no influence of ASC glutathionylation on activation of AIM2 inflammasome or NLR4 inflammasome. Moreover, we showed that LPS-poly(dA:dT)-induced ASC oligomerization and LPS-Flagellin-induced ASC oligomerization were predominantly in mitochondrial fraction (Fig. S5, D and E), where glutathionylated ASC was absent (Fig. 5 B). GSTO1 deficiency reduced the LPS-poly(dA:dT)-induced and LPS-Flagellin-induced ASC oligomerization in mitochondrial fraction (Fig. S5, D and E), confirming the requirement of GSTO1 for activating AIM2 inflammasome and NLR4 inflammasome. Together, these findings demonstrate that GSTO1 promotes activation of AIM2 inflammasome and NLR4 inflammasome via other mechanisms rather than ASC de-glutathionylation, and ASC de-glutathionylation is not required for activating these inflammasomes.

ASC^{C171A} mutant leads to NLRP3 inflammasome-dependent hyperinflammation

Our findings indicate that de-glutathionylation of ASC in response to mitochondrial ROS serves as a derepression signal triggering the activation of NLRP3 inflammasome. It is well known that NLRP3 inflammasome activator as signal 2 induces mitochondrial ROS (Mills et al., 2016) and promotes NLRP3 inflammasome assembly (Amores-Iniesta et al., 2017). Due to the

absence of glutathionylated ASC in *Asc^{C171A}* BMDMs, mitochondrial ROS was not required for NLRP3 inflammasome activation (Fig. 4, I and J). Consistently, we found that oligomerization of ASC and processing of pro-caspase-1 and pro-IL-1 β were induced by LPS alone without the presence of ATP in *Asc^{C171A}* BMDMs (Fig. 7 A). Via inhibiting NLRP3 with Oridonin or knocking down *Nlrp3*, we further proved that IL-1 β production induced by LPS alone in these *Asc^{C171A}* BMDMs was NLRP3 inflammasome dependent (Fig. 7, B and C). In *Asc^{C171A}* BMDMs, adding ATP further increased IL-1 β production (Fig. 7, B and C), indicating that ATP as signal 2 may regulate other pathways in addition to ASC de-glutathionylation. Together, our findings suggest that without repressive effect of ASC glutathionylation, NLRP3 inflammasome could be activated by signal 1 alone, implying hyperactivation of NLRP3 inflammasome. Moreover, when LPS was injected into *Asc^{C171A}* and *Asc^{wt}* mice to induce septic shock, the *Asc^{C171A}* mice produced higher levels of proinflammatory cytokines including IL-1 β , IL-6, and TNF- α , and the production of these cytokines was abrogated by NLRP3 inhibitor Oridonin (Fig. 7 D). These findings exhibited a NLRP3 inflammasome-dependent hyperinflammatory phenotype of *Asc^{C171A}* mice. In line with the hyperinflammation caused by LPS injection, *Asc^{C171A}* mice exhibited higher mortality than *Asc^{wt}* mice (Fig. 7 E). Additionally, when NLRP3 specific activator MSU was injected into joints of *Asc^{wt}* mice and *Asc^{C171A}* mice to induce arthritis, we found that *Asc^{C171A}* mice showed more severe joint swelling than *Asc^{wt}* mice, and NLRP3 inhibitor MCC950 significantly reduced joint swelling in both groups (Fig. 7, F and G). Consistently, joints from the MSU-injected *Asc^{C171A}* mice released higher amounts of IL-1 β than joints from MSU-injected *Asc^{wt}* mice when cultured ex vivo, and IL-1 β production was inhibited by MCC950 (Fig. 7 H). We also measured IL-1 β production in sera from these MSU-injected *Asc^{C171A}* and *Asc^{wt}* mice and confirmed the higher level of IL-1 β in *Asc^{C171A}* mice (Fig. 7 H). Again, MCC950 inhibited MSU-induced IL-1 β production in sera of these mice (Fig. 7 H). These results demonstrate the hyperinflammation in *Asc^{C171A}* mice after activating NLRP3 inflammasome. It is possible that glutathionylation of ASC serves as a brake to prevent NLRP3 inflammasome-related hyperinflammation in vivo.

Discussion

Despite significant progress in understanding NLRP3 inflammasome activation, the mechanisms governing NLRP3 inflammasome activation and prevention of excessive inflammation are largely unknown. Our results indicate that glutathionylation of ASC at its cysteine¹⁷¹ residue inhibits ASC oligomerization in the resting state and thereby blocks unwanted activation of NLRP3 inflammasome. This repressive effect is relieved by GSTO1-mediated de-glutathionylation of ASC in response to

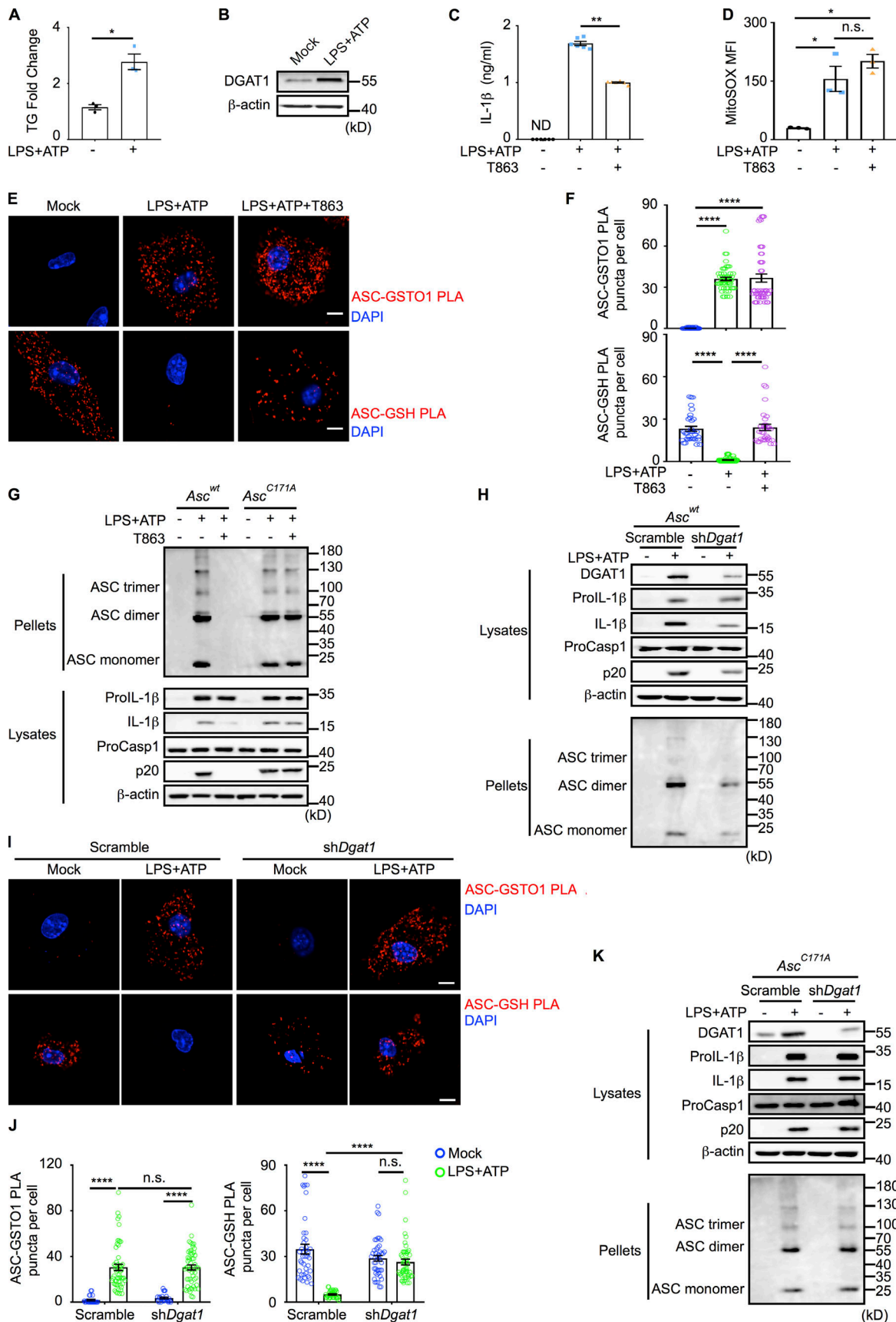


Figure 6. **Triacylglyceride synthesis in ER promotes the deglutathionylation of ASC and the activation of NLRP3 inflammasome.** (A) Fold-change of triacylglyceride (TG) level in BMDMs after LPS+ATP stimulation, measured by liquid chromatography–mass spectrometry ($n = 3$ samples; *, $P < 0.05$ by two-

tailed Mann–Whitney *U* test). **(B)** Immunoblot analysis for DGAT1 in BMDMs with or without LPS-ATP stimulation. **(C and D)** IL-1 β production ($n = 6$ samples, representing three independent experiments; ND, not detected; **, $P < 0.01$ by two-tailed Mann–Whitney *U* test; C) and mitochondrial ROS ($n = 3$ samples, representing three independent experiments; *, $P < 0.05$ by two-tailed Mann–Whitney *U* test; D) from unstimulated and LPS-ATP-stimulated BMDMs in the presence or absence of T863. **(E and F)** Images of ASC–GSTO1 interaction (ASC–GSTO1 PLA) and glutathionylated ASC (ASC–GSH PLA; scale bars, 5 μm); E) and numbers of ASC–GSTO1 PLA puncta and ASC–GSH PLA puncta ($n = 33$ –72 cells from three independent experiments; ****, $P < 0.0001$ by unpaired Student's *t* test; F) in unstimulated and LPS-ATP-stimulated BMDMs with or without T863 treatment. **(G and H)** Immunoblot analysis for ASC oligomerization, pro-IL-1 β , cleaved IL-1 β , pro-caspase-1, and active caspase-1 p20 in unstimulated and LPS-ATP-stimulated *Asc*^{wt} and *Asc*^{C171A} BMDMs, with or without T863 treatment (G), and in unstimulated and LPS-ATP-stimulated *Asc*^{wt} BMDMs, with or without knockdown of *Dgat1* (H). **(I and J)** Images of ASC–GSTO1 interaction (ASC–GSTO1 PLA) and glutathionylated ASC (ASC–GSH PLA; scale bars, 5 μm); I) and numbers of ASC–GSTO1 PLA puncta and ASC–GSH PLA puncta ($n = 26$ –60 cells from three independent experiments; ****, $P < 0.0001$ by unpaired Student's *t* test; J) in unstimulated and LPS-ATP-stimulated *Asc*^{wt} BMDMs, with or without knockdown of *Dgat1*. **(K)** Immunoblot analysis for DGAT1, pro-IL-1 β , cleaved IL-1 β , pro-caspase-1, active caspase-1 p20, and ASC oligomerization in unstimulated or LPS-ATP-stimulated *Asc*^{C171A} BMDMs, with or without knockdown of *Dgat1*. Data are representative of at least three independent experiments (B, E, G–I, and K).

mitochondrial ROS. Thus, deglutathionylation of ASC functions as a major checkpoint for triggering the NLRP3 inflammasome activation. Our finding that GSTO1 promotes NLRP3 inflammasome activation by deglutathionylating ASC rather than other proteins is contrary to those of another study that indicated a role of GSTO1 in deglutathionylating NEK7 (Hughes et al., 2019). It is possible that the NEK7 overexpression strategy used in that study is responsible for the different result. Under stress conditions, glutathionylation of other inflammasome proteins has been reported to regulate inflammasome activation (Meissner et al., 2008). Deficiency of superoxide dismutase 1 inhibits NLRP3 inflammasome activation potentially by increasing the extent of glutathionylation on pro-caspase-1 protein. In the same study, both inhibitory glutathionylation sites and activating glutathionylation sites on overexpressed pro-caspase-1 have been indicated. Stressed conditions might increase the complexity of glutathionylation-based regulation on NLRP3 inflammasome activation. Notably, GSTO1 is not the only factor promoting ASC deglutathionylation in activated BMDMs, as indicated by LPS-ATP stimulation-induced ASC deglutathionylation in GSTO1-deficient BMDMs. Whether glutaredoxins contribute to ASC deglutathionylation in these GSTO1-deficient cells remains to be explored. In the absence of ASC glutathionylation, ATP as signal 2 was not essential for NLRP3 inflammasome activation. This result is particularly interesting in light of a previous study that found NLRP3 inflammasome activation in dendritic cells (DCs) to be signal 2 independent (Kang et al., 2013). In addition to the higher levels of pro-IL-1 β and NLRP3 in DCs than in macrophages, distinct ASC glutathionylation/deglutathionylation in DCs might also make a contribution. As shown by the structural simulations, conjugation of GSH to ASC cysteine¹⁷¹ interfered with ASC–CARD interactions and inhibited ASC oligomerization. Notably, the ASC–CARD domain also binds CARD domain of pro-caspase-1. We did not exclude the possibility that ASC glutathionylation might influence the ASC–pro-caspase-1 interaction as well.

Although the ASC protein has been reported as a cytosolic protein, our results indicated that glutathionylated ASC was enriched at intracellular compartments, particularly at ER, rather than at the cytosol or mitochondria (Fig. 5 B). It is possible that the nonglutathionylated ASC in cytosol and mitochondria makes no/low contribution to NLRP3 inflammasome activation. Indeed, we showed that oligomerized ASC was detected mainly at ER rather than at cytosol or mitochondria while activating

NLRP3 inflammasome (Fig. 5, F and H). These results suggest that other ER-related factors in addition to nonglutathionylated ASC control NLRP3 inflammasome activator-induced ASC oligomerization. A previous study proposed that NLRP3 and ASC may translocate to MAMs after LPS-ATP stimulation (Zhou et al., 2011). In our study, ASC oligomers induced by NLRP3 inflammasome activators were predominantly enriched in the ER fraction that contained no MAMs, as indicated by the absence of FAFL4 (Fig. 5, F and H). Interestingly, AIM2 and NLRC4 inflammasome activators induce ASC oligomerization predominantly at mitochondria where ASC is not glutathionylated. These findings explain the dispensable role of ASC deglutathionylation in activating AIM2 and NLRC4 inflammasomes. Therefore, GSTO1-promoted ASC deglutathionylation is not generally required for activation of all ASC-dependent inflammasomes.

ASC deglutathionylation induced by NLRP3 inflammasome activators is promoted by mitochondrial ROS and triacylglyceride synthesis at different steps, in line with reported essential roles of ROS and fatty acid synthesis in activating NLRP3 inflammasome (Moon et al., 2015). Given the previously reported metabolic control on priming process, activation of NLRP3 inflammasome is regulated by cellular metabolism at multiple steps. Still, further studies are required to understand the mechanisms of how triacylglyceride controls GSTO1-mediated ASC deglutathionylation.

It is well known that NLRP3 inflammasome closely relates to autoimmune diseases and inflammatory diseases, including experimental autoimmune encephalitis (Inoue et al., 2012), colitis (Bauer et al., 2010), and insulin resistance (Vandanmagsar et al., 2011). Unlike GSTO1 deficiency, *Asc*^{C171A} mutant results in hyperinflammation in mouse models. Therefore, we propose a link between GSTO1, deglutathionylation of ASC, and inflammasome-related diseases. Whether the differential expression and/or genetic polymorphisms in *Gsto1* or *Asc* may relate to these inflammatory diseases remains unclear. Further studies are required to explore the roles of this regulatory pathway in human diseases and evaluate its potential as a drug target.

Materials and methods

Mice

Gsto1^{-/-} mice were generated by deleting exons 1–4. *Asc*^{C171A} mice expressing *Asc*^{C171A} mutant were generated using CRISPR/Cas9-mediated genome editing to replace the cysteine at position 171

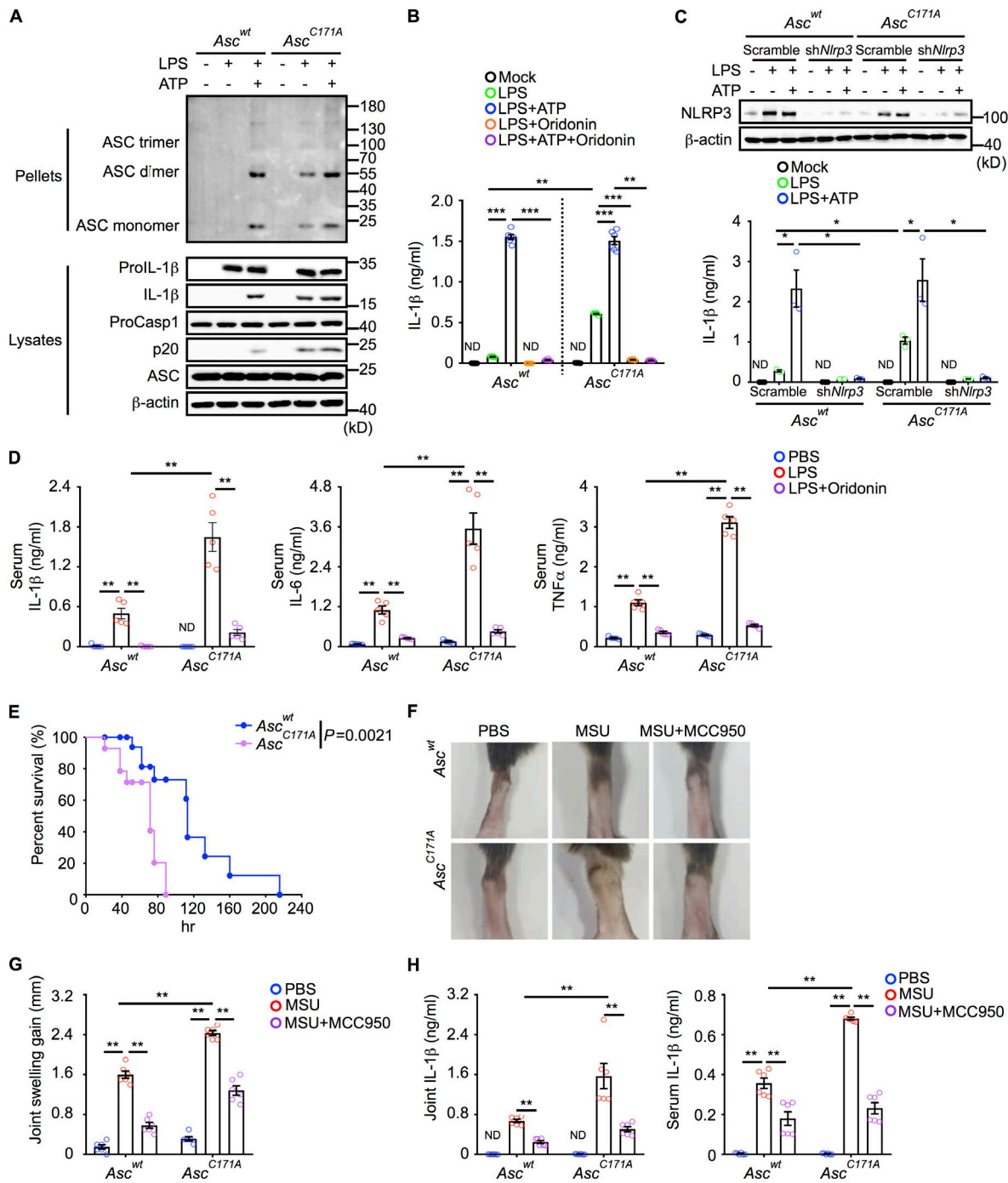


Figure 7. ASC^{C171A} leads to NLRP3 inflammasome-dependent hyperinflammation. (A) Immunoblot analysis for ASC oligomerization, pro-IL-1 β , cleaved IL-1 β , pro-caspase-1, and active caspase-1 p20 in LPS-primed *Asc^{wt}* and *Asc^{C171A}* BMDMs followed with or without ATP stimulation (representative of three independent experiments). (B) Production of IL-1 β from LPS-primed *Asc^{wt}* and *Asc^{C171A}* BMDMs with or without of ATP or Oridonin treatment ($n = 6$ samples, representing three independent experiments; ND, not detected; **, $P < 0.01$; ***, $P < 0.001$ by two-tailed Mann-Whitney U test). (C) NLRP3 level and supernatant IL-1 β from LPS-primed *Asc^{wt}* and *Asc^{C171A}* BMDMs with or without knockdown of *Nlrp3*, in the presence or absence of ATP stimulation ($n = 3$ samples, representing three independent experiments; ND, not detected; *, $P < 0.05$ by two-tailed Mann-Whitney U test). (D) IL-1 β , IL-6, and TNF- α in sera from *Asc^{wt}* and *Asc^{C171A}* mice after LPS injection, with or without Oridonin treatment ($n = 5$ mice; ND, not detected; **, $P < 0.01$ by two-tailed Mann-Whitney U test). (E) Survival rate of *Asc^{wt}* and *Asc^{C171A}* mice after LPS injection ($n = 10$ mice; $P = 0.0021$ by log-rank test). (F-H) Picture of joints (F), the joint swelling gain (G), and IL-1 β from joints and sera (H) of *Asc^{wt}* and *Asc^{C171A}* mice after injecting PBS or MSU for 24 h, with or without MCC950 treatment ($n = 6$ mice from two independent experiments; **, $P < 0.01$ by two-tailed Mann-Whitney U test).

with alanine in the third exon of ASC. All mice used were on the C57BL/6J background and were 8–12 wk old. Cohoused littermate controls were used in our experiments. Mice were housed under specific pathogen-free conditions. Food and water were available ad libitum. All animal procedures were approved by the Animal Care and Use Committee of University of Science and Technology of China, and all experiments were performed in accordance with approved guidelines.

To induce arthritis, MSU (Sigma-Aldrich, U0881) was injected into the joints of *Gsto1^{+/+}*, *Gsto1^{-/-}*, *Asc^{wt}*, and *Asc^{C17A}* mice at a dose of 0.5 mg per mouse, and size of joint was measured at different time points. MCC950 (Selleckchem, S8930) was injected into the joints at a dose of 50 mg kg⁻¹. To measure the production of IL-1 β from the joints, patellae from these mice were isolated after 24 h and cultured in 200 μ l Opti-MEM (Gibco) for 1 h. To induce lethal septic shock, mice were challenged i.p. with LPS (Sigma-Aldrich, L4391) at a dose of 15 mg kg⁻¹. Oridonin (Selleck) was injected into mice at a dose of 20 mg kg⁻¹. To measure the production of IL-1 β , IL-6, and TNF- α , sera were collected from these mice after 24 h.

Cell culture and stimulation

To induce BMDMs, bone marrow cells were cultured in DMEM (Gibco) supplemented with 10% FBS (Biological Industries), 50 μ M β -mercaptoethanol (Sigma-Aldrich), and 50 μ g ml⁻¹ M-CSF (Novus Biologicals) for 5–6 d. For NLRP3 inflammasome activation, BMDMs or peritoneal macrophages were primed with 50 ng ml⁻¹ LPS (Sigma-Aldrich, L4391) for 4 h and then stimulated with 3 mM ATP (Sigma-Aldrich, A2383) or 5 μ M Nigericin (Sigma-Aldrich, N7143) for 30 min, with 150 μ g ml⁻¹ MSU (Sigma-Aldrich, U0881) for 3 h, or with 45 μ g ml⁻¹ CL097 (InvivoGen, tlr-c97) or 45 μ g ml⁻¹ imiquimod (InvivoGen, tlr-imq) for 1 h. To inhibit the enzyme activity of GSTO1, BMDMs were treated with ML175 (AOBIOUS AOB1209) at 4 μ M. To inhibit the production of mitochondrial ROS, BMDMs were treated with Mito-TEMPO (Enzo ALX-430-150) at 0.5 or 1 mM, or with MitoQ (MedChemExpress, HY-100116A) at 1 μ M. To inhibit the production of ER ROS, BMDMs were treated with EN460 (MedChemExpress, HY-12837) at 10 μ M. To inhibit activation of NLRP3 inflammasome, BMDMs were treated with Oridonin (Selleckchem, S2335) at 2 mM. To inhibit the synthesis of triacylglyceride, BMDMs were treated with T863 (MedChemExpress, HY-32219) at 10 μ M. To inhibit the synthesis of cholesterol, BMDMs were treated with Simvastatin (MedChemExpress, HY-17502) at 10 or 20 μ M. These inhibitors were added to cells together with LPS. IL-1 β , IL-6, and TNF- α in supernatants and sera were measured with cytometric beads array kit.

Antibodies

Anti-ASC (Cell Signaling Technology, 67824, 1:1,000), anti-NLRP3 (Cell Signaling Technology, 15101, 1:1,000), anti-cleaved IL-1 β (Cell Signaling Technology, 52718, 1:1,000), anti-pro-IL-1 β (Cell Signaling Technology, 31202, 1:1,000), anti-DGAT1 (Gene-Protein Link, 1:1,000), anti- β -actin (Cell Signaling Technology, 3700, 1:2,000), anti-pro-caspase-1/cleaved caspase-1 p20 (AdipoGen Life Sciences, AG-20B-0042, 1:1,000), anti-NEK7

(Santa Cruz, sc-50756, 1:1,000), anti-GSTO1 (Proteintech, 15124-1-AP, 1:1,000), anti-GSH (ViroGen, 101-A, 1:1,000), anti-calnexin (LifeSpan Biosciences, LS-B9772-200, 1:1,000), anti-FACLA (ABclonal, A20414, 1:1,000), peroxidase-conjugated donkey anti-rabbit IgG (Jackson ImmunoResearch, 111-035-144, 1:5,000), anti-mouse IgG (Jackson ImmunoResearch, 111-035-146, 1:5,000), peroxidase-conjugated donkey anti-goat IgG (Abcam, ab97110, 1:5,000), and Alexa Fluor 488-conjugated chicken anti-goat IgG (Invitrogen, 21467, 1:1,000) were used in our experiments.

Coimmunoprecipitation and ASC oligomerization assay

In coimmunoprecipitation experiments, cells were harvested and lysed with cell lysis buffer (50 mM Tris, pH 8.0, 280 mM NaCl, 0.5% NP-40, 0.2 mM EDTA, 2 mM EGTA, 10% glycerol, 1 mM dithiothreitol, and protease inhibitor cocktail), and then centrifuged at 13,000 *g* at 4°C for 10 min. The supernatants were incubated with Dynabeads Protein G (Invitrogen) and corresponding antibodies overnight at 4°C. The proteins in the precipitated complexes were analyzed by Western blot. To measure the glutathionylation of proteins in NLRP3 inflammasome, anti-ASC, anti-NLRP3, anti-NEK7, and anti-pro-caspase1 antibodies were used to detect corresponding proteins coimmunoprecipitated with anti-GSH antibody, respectively. To detect the oligomerization of ASC, cells were lysed with a lysis buffer (20 mM Hepes-KOH, pH 7.5, 150 mM KCl, 1% NP-40, 0.1 mM PMSF, and protease inhibitor cocktail) and centrifuged at 6,000 rpm at 4°C for 10 min. The pellets were resuspended in CHAPS buffer (20 mM Hepes-KOH, pH 7.5, 5 mM MgCl₂, 0.5 mM EGTA, and 0.1% CHAPS). The resuspended pellets were cross-linked with BS³ cross-linker (Thermo Fisher Scientific) at 4 mM concentration for 30 min at room temperature, and then were dissolved in SDS sample buffer. To detect ASC oligomerization in distinct cell fractions, mitochondria, ER, and cytosol were isolated from BMDMs using Endoplasmic Reticulum Isolation kit (Sigma-Aldrich). Cell fractions were then cross-linked with BS³ cross-linker (Thermo Fisher Scientific) as described.

Immunofluorescence staining and PLA

BMDMs on glass-bottom dishes were washed and fixed with 4% paraformaldehyde in PBS buffer for 15 min and then permeabilized using 0.1% Triton X-100 for 15 min. After blocking with 2% BSA for 1 h, cells were incubated with primary antibodies overnight at 4°C, followed by staining with secondary antibodies. Nuclei were stained with DAPI. To stain the mitochondria, BMDMs were added to prewarmed (37°C) staining solution containing Mito-Tracker probe (Invitrogen) using a working concentration of 400 nM for 30 min under growth conditions. Cells were imaged by an LSM 880 laser scanning microscope (Zeiss).

To detect glutathionylated ASC and ASC-GSTO1 interaction in situ, PLA was performed using Duolink In situ PLA kit (Sigma-Aldrich). Briefly, BMDMs on glass-bottom dishes were fixed and permeabilized as described. Cells were then incubated with primary antibodies against the two targets at 4°C overnight. After washing, a pair of PLA probe-labeled secondary antibodies targeting the primary antibodies were added to cells to allow signal amplification only if the two targets interacted

with each other. To view the ASC-ASC interaction in situ with the PLA approach, two distinct ASC-specific primary antibodies were used to target the different ASC proteins simultaneously, followed by incubation with two PLA probe-labeled secondary antibodies, and only interaction between two ASC proteins binding distinct primary antibodies could generate PLA signal. To validate the staining method, two distinct primary antibodies against ASC were added to stimulated cells sequentially, with an interval long enough to ensure blocking ASC by the first antibody, followed by incubation with two PLA probe-labeled secondary antibodies. The absence of PLA signal indicated that two primary antibodies competed for binding same ASC protein. Therefore, we could exclude the possibility of binding two distinct primary antibodies at the same ASC protein in ASC oligomers. Nuclei were stained with DAPI. Confocal image acquisition was performed using an LSM 880 laser scanning microscope (Zeiss). Quantification of PLA signal was performed with ImageJ software.

Knockdown of *Dgat1*, *Gsto1*, and *Nlrp3*

293T cells were transfected with the vector containing shRNA *Dgat1* (5'-CCGGGCTGAGTCTGTCACC-3'; 6 μ g), shRNA *Gsto1* (5'-CCGGCCTTCTATGGTTGATTATCTTCTCGAGAAGATAATCAA CCATAGAA-3'), and shRNA *Nlrp3* (5'-CCGGCCGGCCTTACTTCA ATCTGTCTCGAGAACAGATTGAAGTAAGGCC-3'; 6 μ g) along with PMD2.G (2 μ g) and PsPAX2 (4 μ g), respectively. The lentivirus-containing media were collected and passed through 0.45- μ m filters after 48 h. BMDMs were seeded on 6-well plates with 80×10^4 cells per well, and the lentivirus-containing medium was then added to cells for 48 h to knock down *Dgat1*, *Gsto1*, and *Nlrp3*. Scrambled shRNA (5'-TTCTCCGAACGTGTACGT-3') was used as a negative control.

MD simulations

The cryo-EM structure of human ASC-CARD filament (PDB accession number 6NIH; Li et al., 2018) was used to generate monomeric, dimeric, and 16mer filament structures of mouse ASC-CARD with the MUTATE plugin in VMD (Humphrey et al., 1996). Only the dimeric configuration with residue cysteine¹⁷¹ located at the binding interface is considered. The initial positions of GSH in monomeric and dimeric structure were obtained by docking to the vicinity of residue cysteine¹⁷¹ with Autodock Vina (Trott and Olson, 2010), and the docking result that favored the formation of cysteine-GSH disulfide bond was selected. The initial positions of GSH in 16mer filament structure were modeled from that in the docked dimeric structure. These initial models with or without GSH conjugation were then processed with VMD PSFGEN plugin to add hydrogen and other missing atoms. The resulting systems were solvated in rectangular water boxes with a TIP3P water model. K⁺ and Cl⁻ ions were then added to these solvated systems to neutralize the systems and maintain salt concentration at 150 mM.

All simulations were performed with NAMD2 (Phillips et al., 2005) software using CHARMM36m additive protein forcefield with CMAP correction (MacKerell et al., 1998) under the periodic boundary condition. The force field of GSH was generated from CHARMM general forcefield (CGenFF; Vanommeslaeghe

et al., 2010). All systems underwent energy minimization with four steps: (1) 10,000 steps with the heavy atoms of proteins fixed; (2) 10,000 steps with the backbone atoms of proteins fixed; (3) 10,000 steps with the backbone atoms of proteins fixed; and (4) 10,000 steps with all atoms free. Then each system was equilibrated for 10 ns with 1-fs time steps. Finally, production simulations were performed with 2-fs time steps under rigid bond algorithms, and the snapshots were saved every 100 ps for further analysis. For each system, the temperature was controlled at 310 K by Langevin dynamics, and the pressure was maintained at 1 atm by the Nosé-Hoover Langevin piston method during the simulation. Particle mesh Ewald summation was used for computing the electrostatic interactions, and a 12-Å cutoff with 10-12-Å smooth switching was used for short-range nonbonded interactions. The system preparations, trajectory analyses, and graphic illustrations were performed with VMD.

Activation of AIM2 inflammasome, NLR4 inflammasome, and Pyrin inflammasome

For AIM2 inflammasome activation, BMDMs were primed with 50 ng ml⁻¹ LPS (Sigma-Aldrich, L4391) for 4 h and then stimulated by 1 μ g ml⁻¹ poly(dA:dT) (InvivoGen, tlr1-patn-1) transfection for 4 h. For NLR4 inflammasome activation, BMDMs were primed with 50 ng ml⁻¹ LPS (Sigma-Aldrich, L4391) for 4 h and then stimulated with 100 nM *Flagellin* for 6 h. For Pyrin inflammasome activation, BMDMs were primed with 50 ng ml⁻¹ LPS (Sigma-Aldrich, L4391) for 4 h and then stimulated with 500 ng ml⁻¹ TcdB (Abcam, ab124001) for 1 h.

Statistical analysis

Statistical analyses were performed with Mann-Whitney *U* test, unpaired Student's *t* test, and log-rank test, using GraphPad Prism 8.0.1 software. Unpaired Student's *t* test was used for normally distributed parameters in two unpaired groups, Mann-Whitney *U* test was used for non-normally distributed parameters in two unpaired groups, and log-rank test was used for survival analysis. *, *P* < 0.05, **, *P* < 0.01, ***, *P* < 0.001, and ****, *P* < 0.0001 were considered statistically significant.

Online supplemental material

Fig. S1 shows recovery of IL-1 β production in GSTO1-deficient BMDMs by restoring GSTO1 expression. Fig. S2 shows impairment of ASC-CARD assembly by GSH conjugation. Fig. S3 shows GSH-induced reduction of ASC glutathionylation and elevation of ASC oligomerization in ML175-treated BMDMs. Fig. S4 shows the dispensable role of cholesterol synthesis in NLRP3 inflammasome activation. Fig. S5 shows the dispensable role of ASC deglutathionylation in activating AIM2 and NLR4 inflammasomes.

Acknowledgments

This work was supported by National Natural Science Foundation of China (91942310, 81771671, and 91954122), National Key R&D Program of China (2017YFA0505300), and Fundamental Research Funds for the Central Universities (WK9110000149 and WK9100000001).

Author contributions: S. Li, L. Wang, Z. Xu, Y. Huang, R. Xue, T. Yue, L. Xu, H. Zhang, F. Gong, S. Bai, Q. Wu, J. Liu, and B. Lin performed experiments. Y. Xue, P. Xu, J. Hou, X. Yang, T. Jin, R. Zhou, and T. Xu provided materials or discussed experiments and manuscript. J. Lou performed MD simulations. S. Li and L. Bai conceived the idea, designed the experiments, and wrote the manuscript.

Disclosures: The authors declare no competing interests exist.

Submitted: 10 December 2020

Revised: 8 May 2021

Accepted: 17 June 2021

References

- Amores-Iniesta, J., M. Barberà-Cremades, C.M. Martínez, J.A. Pons, B. Revilla-Nuin, L. Martínez-Alarcón, F. Di Virgilio, P. Parrilla, A. Baroja-Mazo, and P. Pelegrin. 2017. Extracellular ATP Activates the NLRP3 Inflammasome and Is an Early Danger Signal of Skin Allograft Rejection. *Cell Rep.* 21:3414–3426. <https://doi.org/10.1016/j.celrep.2017.11.079>
- Bauer, C., P. Duewell, C. Mayer, H.A. Lehr, K.A. Fitzgerald, M. Dauer, J. Tschopp, S. Endres, E. Latz, and M. Schnurr. 2010. Colitis induced in mice with dextran sulfate sodium (DSS) is mediated by the NLRP3 inflammasome. *Gut.* 59:1192–1199. <https://doi.org/10.1136/gut.2009.197822>
- Board, P.G., M. Coggan, G. Chelvanayagam, S. Easteal, L.S. Jermin, G.K. Schulte, D.E. Danley, L.R. Hoth, M.C. Griffor, A.V. Kamath, et al. 2000. Identification, characterization, and crystal structure of the Omega class glutathione transferases. *J. Biol. Chem.* 275:24798–24806. <https://doi.org/10.1074/jbc.M001706200>
- Chung, I.C., C.N. OuYang, S.N. Yuan, H.P. Li, J.T. Chen, H.R. Shieh, Y.J. Chen, D.M. Ojcius, C.L. Chu, J.S. Yu, et al. 2016. Pyk2 activates the NLRP3 inflammasome by directly phosphorylating ASC and contributes to inflammasome-dependent peritonitis. *Sci. Rep.* 6:36214. <https://doi.org/10.1038/srep36214>
- Dick, M.S., L. Sborgi, S. Rühl, S. Hiller, and P. Broz. 2016. ASC filament formation serves as a signal amplification mechanism for inflammasomes. *Nat. Commun.* 7:11929. <https://doi.org/10.1038/ncomms11929>
- Groß, C.J., R. Mishra, K.S. Schneider, G. Médard, J. Wettmarshausen, D.C. Dittlein, H. Shi, O. Gorka, P.A. Koenig, S. Fromm, et al. 2016. K⁺ Efflux-Independent NLRP3 Inflammasome Activation by Small Molecules Targeting Mitochondria. *Immunity.* 45:761–773. <https://doi.org/10.1016/j.immuni.2016.08.010>
- Hornung, V., A. Ablasser, M. Charrel-Dennis, F. Bauernfeind, G. Horvath, D.R. Caffrey, E. Latz, and K.A. Fitzgerald. 2009. AIM2 recognizes cytosolic dsDNA and forms a caspase-1-activating inflammasome with ASC. *Nature.* 458:514–518. <https://doi.org/10.1038/nature07725>
- Hoss, F., J.F. Rodriguez-Alcazar, and E. Latz. 2017. Assembly and regulation of ASC specks. *Cell. Mol. Life Sci.* 74:1211–1229. <https://doi.org/10.1007/s00018-016-2396-6>
- Hughes, M.M., A. Hooftman, S. Angiari, P. Tummala, Z. Zaslona, M.C. Runtzsch, A.F. McGettrick, C.E. Sutton, C. Diskin, M. Rooke, et al. 2019. Glutathione Transferase Omega-1 Regulates NLRP3 Inflammasome Activation through NEK7 Deglutathionylation. *Cell Rep.* 29:151–161.e5. <https://doi.org/10.1016/j.celrep.2019.08.072>
- Humphrey, W., A. Dalke, and K. Schulten. 1996. VMD: visual molecular dynamics. *J. Mol. Graph.* 14:33–38. [https://doi.org/10.1016/0263-7855\(96\)00018-5](https://doi.org/10.1016/0263-7855(96)00018-5)
- Inoue, M., K.L. Williams, M.D. Gunn, and M.L. Shinohara. 2012. NLRP3 inflammasome induces chemotactic immune cell migration to the CNS in experimental autoimmune encephalomyelitis. *Proc. Natl. Acad. Sci. USA.* 109:10480–10485. <https://doi.org/10.1073/pnas.1201836109>
- Kang, T.B., S.H. Yang, B. Toth, A. Kovalenko, and D. Wallach. 2013. Caspase-8 blocks kinase RIPK3-mediated activation of the NLRP3 inflammasome. *Immunity.* 38:27–40. <https://doi.org/10.1016/j.immuni.2012.09.015>
- Li, Y., T.M. Fu, A. Lu, K. Witt, J. Ruan, C. Shen, and H. Wu. 2018. Cryo-EM structures of ASC and NLRC4 CARD filaments reveal a unified mechanism of nucleation and activation of caspase-1. *Proc. Natl. Acad. Sci. USA.* 115:10845–10852. <https://doi.org/10.1073/pnas.1810524115>
- Lu, A., V.G. Magupalli, J. Ruan, Q. Yin, M.K. Atianand, M.R. Vos, G.F. Schröder, K.A. Fitzgerald, H. Wu, and E.H. Egelman. 2014. Unified polymerization mechanism for the assembly of ASC-dependent inflammasomes. *Cell.* 156:1193–1206. <https://doi.org/10.1016/j.cell.2014.02.008>
- MacKerell, A.D., D. Bashford, M. Bellott, R.L. Dunbrack, J.D. Evanseck, M.J. Field, S. Fischer, J. Gao, H. Guo, S. Ha, et al. 1998. All-atom empirical potential for molecular modeling and dynamics studies of proteins. *J. Phys. Chem. B.* 102:3586–3616. <https://doi.org/10.1021/jp973084f>
- McKee, C.M., and R.C. Coll. 2020. NLRP3 inflammasome priming: A riddle wrapped in a mystery inside an enigma. *J. Leukoc. Biol.* 108:937–952. <https://doi.org/10.1002/JLB.3MR0720-513R>
- Meissner, F., K. Molawi, and A. Zychlinsky. 2008. Superoxide dismutase 1 regulates caspase-1 and endotoxin shock. *Nat. Immunol.* 9:866–872. <https://doi.org/10.1038/ni.1633>
- Menon, D., and P.G. Board. 2013. A role for glutathione transferase Omega 1 (GSTO1-1) in the glutathionylation cycle. *J. Biol. Chem.* 288:25769–25779. <https://doi.org/10.1074/jbc.M113.487785>
- Menon, D., A. Innes, A.J. Oakley, J.E. Dahlstrom, L.M. Jensen, A. Brüstle, P. Tummala, M. Rooke, M.G. Casarotto, J.B. Baell, et al. 2017. GSTO1-1 plays a pro-inflammatory role in models of inflammation, colitis and obesity. *Sci. Rep.* 7:17832. <https://doi.org/10.1038/s41598-017-17861-6>
- Miao, E.A., J.V. Rajan, and A. Aderem. 2011. Caspase-1-induced pyroptotic cell death. *Immunol. Rev.* 243:206–214. <https://doi.org/10.1111/j.1600-065X.2011.01044.x>
- Mills, E.L., B. Kelly, A. Logan, A.S.H. Costa, M. Varma, C.E. Bryant, P. Tourlomeousis, J.H.M. Däbritz, E. Gottlieb, I. Latorre, et al. 2016. Succinate Dehydrogenase Supports Metabolic Repurposing of Mitochondria to Drive Inflammatory Macrophages. *Cell.* 167:457–470.e13. <https://doi.org/10.1016/j.cell.2016.08.064>
- Moon, J.S., S. Lee, M.A. Park, I.I. Siempos, M. Haslip, P.J. Lee, M. Yun, C.K. Kim, J. Howrylak, S.W. Ryter, et al. 2015. UCP2-induced fatty acid synthase promotes NLRP3 inflammasome activation during sepsis. *J. Clin. Invest.* 125:665–680. <https://doi.org/10.1172/JCI78253>
- Phillips, J.C., R. Braun, W. Wang, J. Gumbart, E. Tajkhorshid, E. Villa, C. Chipot, R.D. Skeel, L. Kalé, and K. Schulten. 2005. Scalable molecular dynamics with NAMD. *J. Comput. Chem.* 26:1781–1802. <https://doi.org/10.1002/jcc.20289>
- Próchnicki, T., M.S. Mangan, and E. Latz. 2016. Recent insights into the molecular mechanisms of the NLRP3 inflammasome activation. *Fl000 Res.* 5:1469. <https://doi.org/10.12688/fl000research.8614.1>
- Sánchez-Rodríguez, R., F. Munari, R. Angioni, F. Venegas, A. Agnellini, M.P. Castro-Gil, A. Castegna, R. Luisetto, A. Viola, and M. Canton. 2021. Targeting monoamine oxidase to dampen NLRP3 inflammasome activation in inflammation. *Cell. Mol. Immunol.* 18:1311–1313. <https://doi.org/10.1038/s41423-020-0441-8>
- Schmidt, F.I., A. Lu, J.W. Chen, J. Ruan, C. Tang, H. Wu, and H.L. Ploegh. 2016. A single domain antibody fragment that recognizes the adaptor ASC defines the role of ASC domains in inflammasome assembly. *J. Exp. Med.* 213:771–790. <https://doi.org/10.1084/jem.20151790>
- Schroder, K., and J. Tschopp. 2010. The inflammasomes. *Cell.* 140:821–832. <https://doi.org/10.1016/j.cell.2010.01.040>
- Trott, O., and A.J. Olson. 2010. AutoDock Vina: improving the speed and accuracy of docking with a new scoring function, efficient optimization, and multithreading. *J. Comput. Chem.* 31:455–461.
- Vandanmagsar, B., Y.H. Youm, A. Ravussin, J.E. Galgani, K. Stadler, R.L. Mynatt, E. Ravussin, J.M. Stephens, and V.D. Dixit. 2011. The NLRP3 inflammasome instigates obesity-induced inflammation and insulin resistance. *Nat. Med.* 17:179–188. <https://doi.org/10.1038/nm.2279>
- Vanommeslaeghe, K., E. Hatcher, C. Acharya, S. Kundu, S. Zhong, J. Shim, E. Darian, O. Guvench, P. Lopes, I. Vorobyov, and A.D. Mackerell Jr. 2010. CHARMM general force field: A force field for drug-like molecules compatible with the CHARMM all-atom additive biological force fields. *J. Comput. Chem.* 31:671–690.
- Wieckowski, M.R., C. Giorgi, M. Liebedzinska, J. Duszynski, and P. Pinton. 2009. Isolation of mitochondria-associated membranes and mitochondria from animal tissues and cells. *Nat. Protoc.* 4:1582–1590. <https://doi.org/10.1038/nprot.2009.151>
- Xu, H., J. Yang, W. Gao, L. Li, P. Li, L. Zhang, Y.N. Gong, X. Peng, J.J. Xi, S. Chen, et al. 2014. Innate immune sensing of bacterial modifications of Rho GTPases by the Pyrin inflammasome. *Nature.* 513:237–241. <https://doi.org/10.1038/nature13449>
- Zhao, Y., J. Yang, J. Shi, Y.N. Gong, Q. Lu, H. Xu, L. Liu, and F. Shao. 2011. The NLRC4 inflammasome receptors for bacterial flagellin and type III secretion apparatus. *Nature.* 477:596–600. <https://doi.org/10.1038/nature10510>
- Zhou, R., A.S. Yazdi, P. Menu, and J. Tschopp. 2011. A role for mitochondria in NLRP3 inflammasome activation. *Nature.* 469:221–225. <https://doi.org/10.1038/nature09663>

Supplemental material

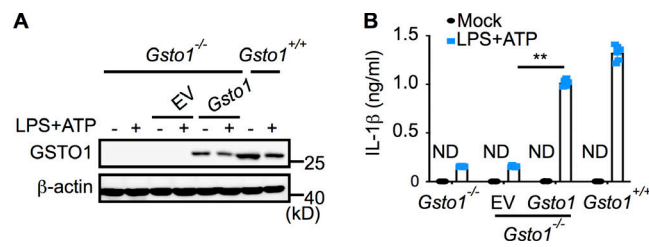


Figure S1. **Recovery of GSTO1 restores IL-1 β production in GSTO1-deficient BMDMs.** (A and B) Immunoblot analysis for GSTO1 (representative of two independent experiments; A) and IL-1 β production ($n = 6$ samples, representing of two independent experiments; ND, not detected; **, $P < 0.01$ by two-tailed Mann-Whitney U test; B) from LPS-ATP-stimulated *Gsto1*^{+/+} BMDMs and *Gsto1*^{-/-} BMDMs transfected with empty virus (EV) or *Gsto1*-virus.

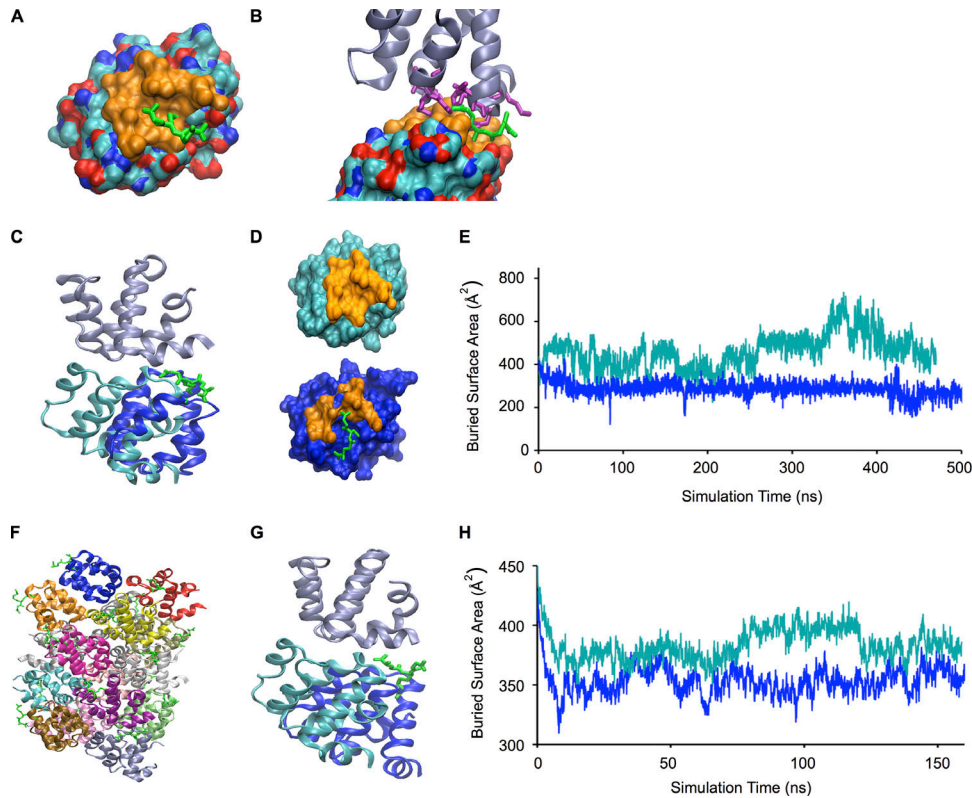


Figure S2. **GSH conjugation impairs ASC-CARD assembly.** (A) Surface profile of ASC-CARD domain. The cysteine¹⁷¹ interaction interface is shown in orange, and a representative GSH location obtained by MD simulation is shown in green. (B) ASC-CARD dimeric structure. GSH (green) clashes heavily with the other ASC-CARD domain (gray cartoon representation with residues located at the binding interface shown in purple). (C) GSH (green) conjugation induces large conformational change at the cysteine¹⁷¹ binding interface in ASC-CARD dimer. After one ASC-CARD domain (gray) is superimposed, rotation from the cryo-EM structure without GSH (cyan) to the MD simulated structure with GSH conjugation (blue) can be clearly observed. (D) Surface area of binding interface (yellow) of the cryo-EM structure (top, cyan) and the simulated structure with GSH conjugation (bottom, blue). (E) Time courses of the buried surface area in the ASC-CARD dimer with (blue) or without (cyan) the GSH conjugation. (F) A representative MD snapshot of GSH-conjugated ASC-CARD 16mer filament. (G) Change of a representative ASC-CARD cysteine¹⁷¹ binding interface in the MD simulation of ASC-CARD 16mer filament upon GSH conjugation. Rotation from the cryo-EM structure without GSH (cyan) to the MD simulated structure with GSH conjugation (blue). (H) Time courses of the average buried surface area in ASC-CARD 16mer filament at the cysteine¹⁷¹ binding interface with (blue) or without (cyan) GSH conjugation.

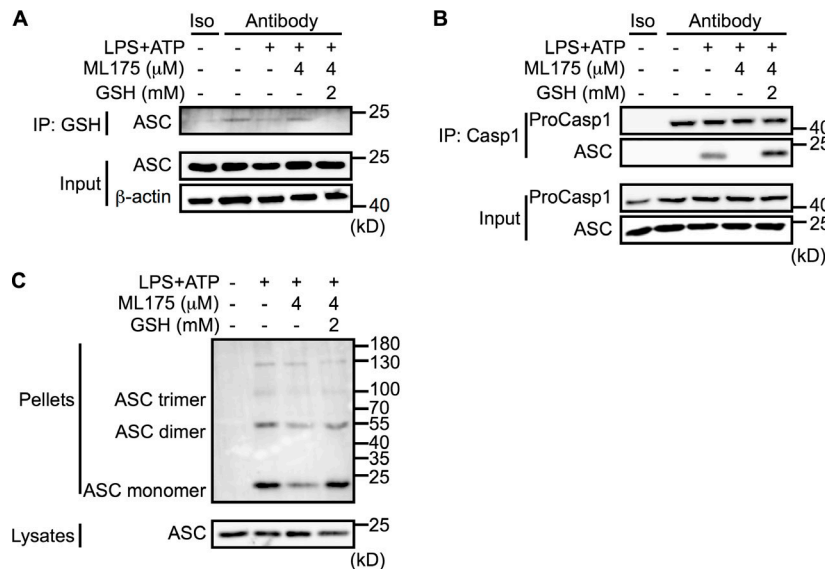


Figure S3. **GSH reduces ASC glutathionylation and rescues ASC oligomerization in ML175-treated BMDMs upon activation of NLRP3 inflammasome.** (A-C) Glutathionylation of ASC (A), coimmunoprecipitation of ASC and pro-caspase-1 (B), and oligomerization of ASC (C) in LPS-ATP-stimulated BMDMs treated with ML175 alone or with the combination of ML175 and GSH as indicated. Data are representative of three independent experiments (A-C).

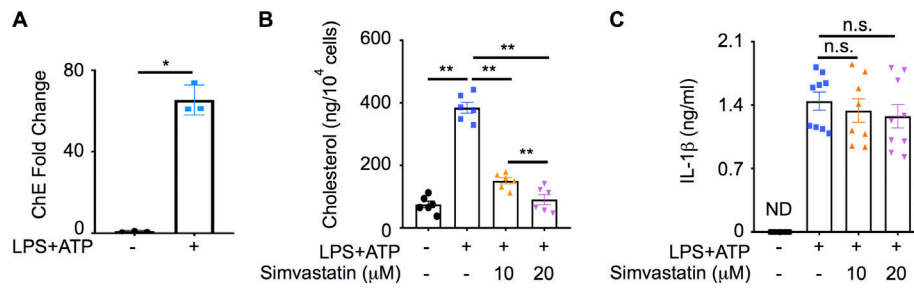


Figure S4. **The synthesis of cholesterol is not required for NLRP3 inflammasome activation.** **(A)** Fold-change of the cholesterol (ChE) level in BMDMs after LPS-ATP stimulation, measured by liquid chromatography–mass spectrometry ($n = 3$ samples; *, $P < 0.05$ by two-tailed Mann–Whitney U test). **(B)** Total cholesterol level in unstimulated and LPS-ATP–stimulated BMDMs with or without Simvastatin treatment at indicated doses ($n = 6$ samples from two independent experiments; **, $P < 0.01$ by two-tailed Mann–Whitney U test). **(C)** IL-1 β production from unstimulated and LPS-ATP–stimulated BMDMs with or without Simvastatin treatment at indicated doses ($n = 8$ –9 samples from three independent experiments; ND, not detected).

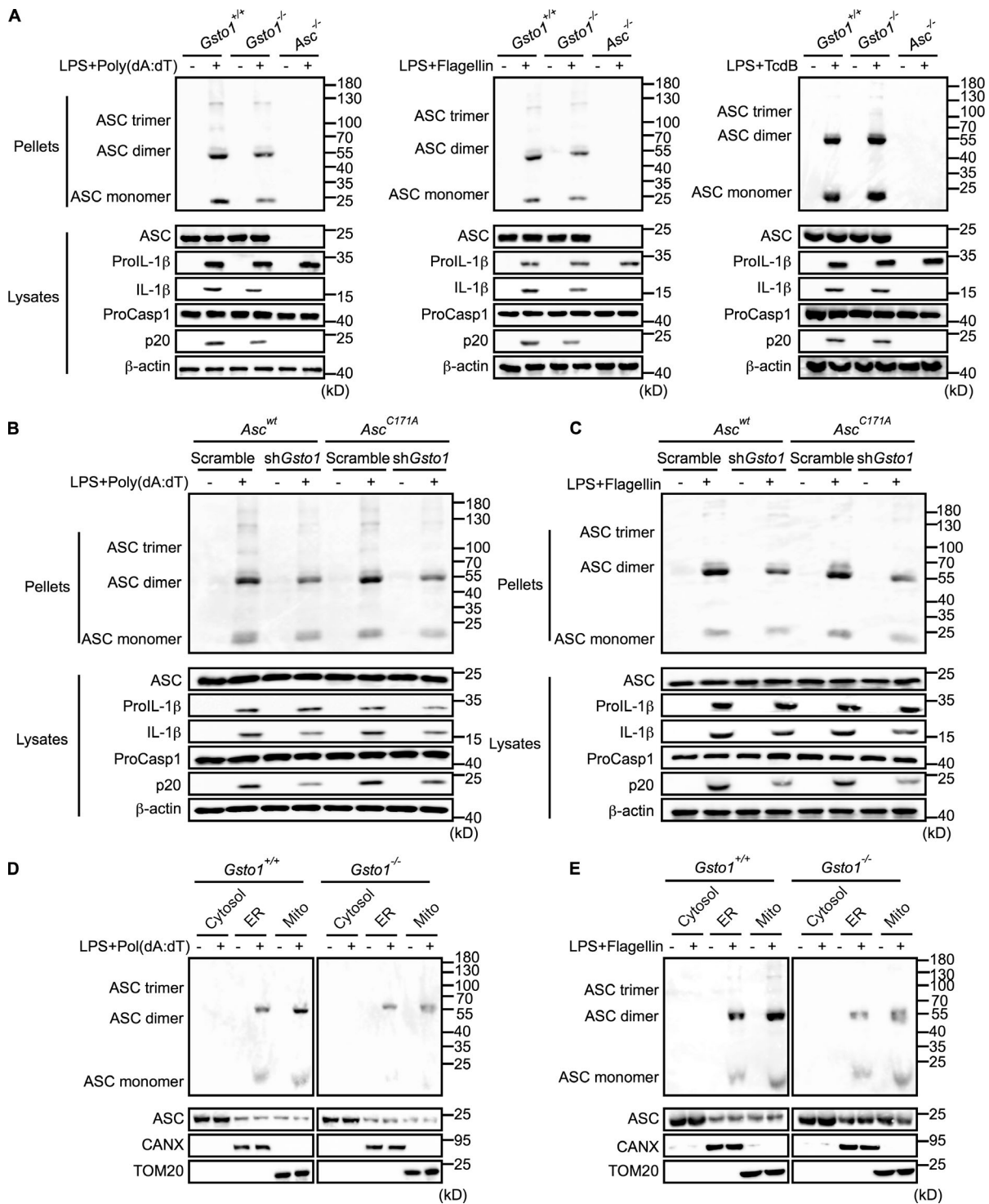


Figure S5. **Deglutathionylation of ASC is not required for activating other inflammasomes.** (A) Immunoblot analysis for ASC oligomerization, pro-IL-1 β , cleaved IL-1 β , pro-caspase-1, and active caspase-1 p20 in unstimulated, LPS-poly(dA:dT)-stimulated, LPS-Flagellin stimulated, and LPS-TcdB-stimulated *Gsto1*^{+/+} BMDMs, *Gsto1*^{-/-} BMDMs, and *Asc*^{-/-} BMDMs. (B and C) Immunoblot analysis for ASC oligomerization, GSTO1, pro-IL-1 β , cleaved IL-1 β , pro-caspase-1, and active caspase-1 p20 in unstimulated, LPS-poly(dA:dT)-stimulated (B), and LPS-Flagellin stimulated (C) *Asc*^{wt} BMDMs and *Asc*^{C171A} BMDMs, transfected with scrambled shRNA (Scramble) or shRNA *Gsto1* (sh*Gsto1*). (D and E) Immunoblot analysis for ASC oligomerization in cytosolic, ER, and mitochondrial fractions from *Gsto1*^{+/+} BMDMs and *Gsto1*^{-/-} BMDMs, with or without LPS-poly(dA:dT) stimulation (D) and LPS-Flagellin stimulation (E). Data are representative of at least three independent experiments (A-E).